Study on Functions of the Heterochromatin Factor Epe1 to Regulate Epigenetic Diversification

エピジェネティックな多様化を制御する ヘテロクロマチン因子 Epe1 の機能に関する研究

Laboratory of Bioorganic Chemistry,
Graduate School of Chemical Sciences and Engineering,
Hokkaido University

Masato Sorida

2019

Table of contents

List of abbreviations

5-FOA	5-fluoroorotic acid
5mC	5-methyl-cytosine
AIR	5-aminoimidazole ribotide
Atf1	cyclic AMP-dependent Transcription Factor 1
CAIR	4-carboxy-5-aminoimidazole ribotide
CD	chromo domain
CDS	coding sequence
ChIP/ChIP-seq	chromatin immunoprecipitation/ChIP-sequencing
CK2	casein kinase II
Clr4	Cryptic Loci Regulator 4
CLRC complex	Clr4-Rik1-Cul4 complex
co-IP	co-immunoprecipitation
DNA	deoxyribonucleic acid
DSR	determinant of selective removal
dTTP	deoxythymidine triphosphate
dUMP	deoxyuridine monophosphate
Epe1	Enhancer of Position Effect 1
Gal4DBD	Gal4 DNA-binding domain
H3K4	histone H3 lysine 4
H3K9	histone H3 lysine 9
H3K9me	methylation of histone H3 at lysine 9
H3K9me2	di-methylation of histone H3 at lysine 9
H3K9me3	tri-methylation of histone H3 at lysine 9
H3K27	histone H3 lysine 27
HOOD	heterochromatin domain
HP1	Heterochromatin Protein 1
IMP	inosine monophosphate
imr	inner most repeat
IR	inverted repeat (*IR* at centromere is called *IRC*)
Is	heterochromatin island
JHDM1	JmjC domain-containing histone demethylase 1

JmjC domain	Jumonji C-terminal domain
JMJD2	Jumonji domain 2
KDM2	lysine (K)-specific histone demethylase 2
MAT locus	mating-type locus
NLS	nuclear localization signal
OE	overexpression
otr	outer repeat
Paf1C	RNA polymerase-associated factor 1 complex
PCR/qPCR	polymerase chain reaction/quantitative PCR
PHF2	Plant Homeodomain Finger 2
PIER	pause-induced ectopic heterochromatic region
PKA	Protein Kinase A
rDNA	ribosomal DNA
Rdp1	RNA-directed RNA Polymerase 1
RITS complex	RNA-induced initiation of transcriptional gene silencing (RNA-induced transcriptional silencing) complex
RNA	ribonucleic acid
RNAi	RNA interference
RNAPII	RNA polymerase II
RT	reverse transcription
SAGA complex	Spt-Ada-Gcn5 acetyltransferase complex
siRNA	small interfering RNA
subtel3R	right subtelomere of chromosome III
Swi6	Switching 6
Taz1	Telomere-associated in *Schizosaccharomyces pombe*
TetO/TetR	tetracycline operator/tetracycline repressor
UMP	uridine monophosphate

Abstract

Post-translational modifications of histones are involved in various cellular events. Methylation of histone H3 at lysine 9 (H3K9me) is a conserved marker for formation of heterochromatin, a transcriptionally silent chromatin structure. Heterochromatin formation is limited to specific genomic loci, but the mechanism for regulating heterochromatin distribution is not fully understood. The fission yeast JmjC domain-containing protein Epe1 localizes to heterochromatin mainly through its physical interaction with Swi6, a homologue of heterochromatin protein 1 (HP1), and directs JmjC-mediated demethylation of H3K9me *in vivo*. However, the physiological role of Epe1 in the control of the genome-wide heterochromatin landscape is unknown. Here, I found that loss of *epe1* (*epe1*Δ) induced a red-white variegated phenotype in a red-pigment accumulation background in contrast to the wild-type strain, which generated uniform red colonies. Analysis of isolated red and white colonies revealed that white colony formation was due to silencing of genes involved in red-pigment accumulation by stochastic ectopic heterochromatin formation. In addition, genome-wide analysis of red- and white-isolated clones revealed that *epe1*Δ resulted in a heterogeneous heterochromatin distribution among clones. These results suggest that multiple potential H3K9me deposition sites exist in the genome and that Epe1 has a genome-wide function to suppress stochastic formation of ectopic heterochromatin. I found that Epe1 had an N-terminal domain distinct from its JmjC domain, which activated transcription in both fission and budding yeasts. Deletion of the N-terminal transcriptional activation (NTA) domain induced ectopic heterochromatin-mediated red-white variegation with lower pink- and white-colony ratio than *epe1*Δ, suggesting that the NTA domain contributes to suppression of ectopic heterochromatin formation in a JmjC-independent mechanism. I introduced a single copy of *epe1* into *epe1*Δ clones harboring ectopic heterochromatin, and found that Epe1 could reduce H3K9me from ectopic heterochromatin. Epe1H297A, a canonical JmjC mutant, suppressed red-white variegation, but entirely failed to remove already-established ectopic heterochromatin, indicating that JmjC domain is not required for suppression of ectopic heterochromatin establishment but essential for removal of established ectopic heterochromatin. I found that some of the ectopic heterochromatin persisted after introduction of a single copy of *epe1*. This persistence was due to a latent H3K9me source embedded in ectopic

heterochromatin. The latent H3K9me source did not initiate deposition of H3K9me in the presence of Epe1, while contributing to maintenance of established heterochromatin. Overexpression of Epe1 depleted the persistent ectopic heterochromatin. These results suggest that the efficiency of Epe1-mediated removal of established ectopic heterochromatin was controlled in a dose-dependent manner and that single copy Epe1 contributed to producing an epigenetic difference. These results suggested that Epe1 prevented stochastic *de novo* deposition of ectopic H3K9me in an NTA-dependent but JmjC-independent manner, while promoting JmjC domain-mediated removal of H3K9me from established ectopic heterochromatin. Taken together, these findings suggest that Epe1 not only limits the distribution of heterochromatin but also controls the balance between suppression and retention of heterochromatin-mediated epigenetic diversification.

I. Introduction

I-1. Chromatin structure and epigenetics

In the eukaryotes, genomic DNA is wrapped around histones and packaged in the cell nucleus (Figure 1A) [1, 2]. Histone is an octamer protein complex, composed of a couple of histone H2A, H2B, H3, and H4 proteins. Each histone protein takes various post-translational modifications, methylation, acetylation, and phosphorylation [3, 4]. Some of them are known to be a key signal inducing cellular events such as gene silencing, transcriptional activation, chromosome segregation, and DNA repair.

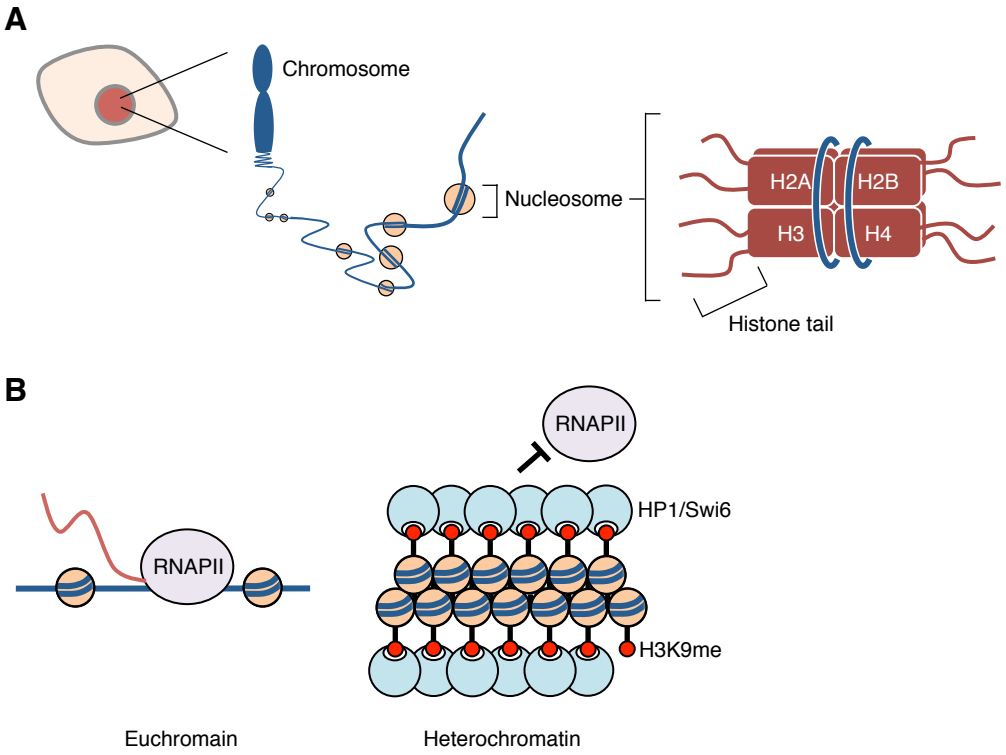

Figure 1. Chromatin structure

(A) The genome DNA is packaged into chromosomes to fit in the nucleus. DNA wrapped around a histone octamer to form a nucleosome. Histone octamer consists of a couple of each of the histone H2A, H2B, H3, and H4 proteins. The N-terminal amino acid region of each histone (known as histone tail) protrudes from the nucleosome core particle and takes various post-translational modifications. (B) Euchromatin is a relaxed chromatin structure, allowing transcription by RNA polymerase II (RNAPII) (left). Heterochromatin is a tight chromatin structure, where HP1 binds to histone H3 with methylation at lysine 9 (H3K9me) (right). Condensed nucleosomes and HP1 proteins limit transcription.

A histone complex and coiled DNA constitute a nucleosome, a basic unit of chromatin (Figure 1A). Chromatin structure is known to be controlled by specific histone modifications. Euchromatin is an open and relaxed chromatin structure, allowing RNA polymerase II to access the genome (Figure 1B). In euchromatic regions, lysine residues of histone H3 and H4 are highly acetylated and typically the residue lysine 4 of histone H3 (H3K4) is tri-methylated at promoter regions of protein-coding genes. These modifications are thought to be transcriptionally active marks.

Heterochromatin is a closed and tight chromatin structure, where highly condensed nucleosomes are believed to keep away transcription machinery from accessing the genome (Figure 1B) [5–7]. In contrast to euchromatin, heterochromatic regions harbor hypo-acetylated histones. Di- and tri-methylation of histone H3 at lysine 9 (H3K9) is a typical and conserved modification of heterochromatin; heterochromatin protein 1 (HP1) binds to methyl-H3K9 and recruits various effectors including silencing factors. In addition, tri-methylation of H3K27 and DNA methylation at cytosine are typical but less conserved heterochromatin marks. These three types of methylation contribute through different mechanisms to formation of the transcriptionally silent chromatin structure heterochromatin. Histone modifications that make a change in chromatin structure and gene expression pattern form a basis of epigenetic regulation, and play an important role in heritable phenotypic alterations independent of a change in DNA sequence [8].

I-2. Heterochromatin assembly in fission yeast

The fission yeast *Schizosaccharomyces pombe* is a well-established model organism to analyze heterochromatin because of its conserved but simplified heterochromatin assembly system. H3K9 methylation is mediated by the sole H3K9 methyltransferase Clr4 [9, 10]. No H3K27 or DNA methyltransferase is identified in fission yeast. The mechanism to assemble heterochromatin requires three separate processes: nucleation, spreading, and maintenance [6, 7]. In nucleation, H3K9me is initially deposited via a mechanism for recruiting Clr4 by factors that bind to specific DNA sequence or transcripts. Clr4 binds to methyl-H3K9 via its chromodomain (CD) to methylate another histone H3 at K9, which allows heterochromatin to spread along chromatin. The nature of Clr4 enables the H3K9me level of assembled heterochromatin to be autonomously maintained. Heterochromatin, in fission yeast, is constitutively formed in centromeric repeats, subtelomeric regions, and the mating-type locus, while the other genomic regions consist almost entirely of euchromatin (Figure 2A) [11].

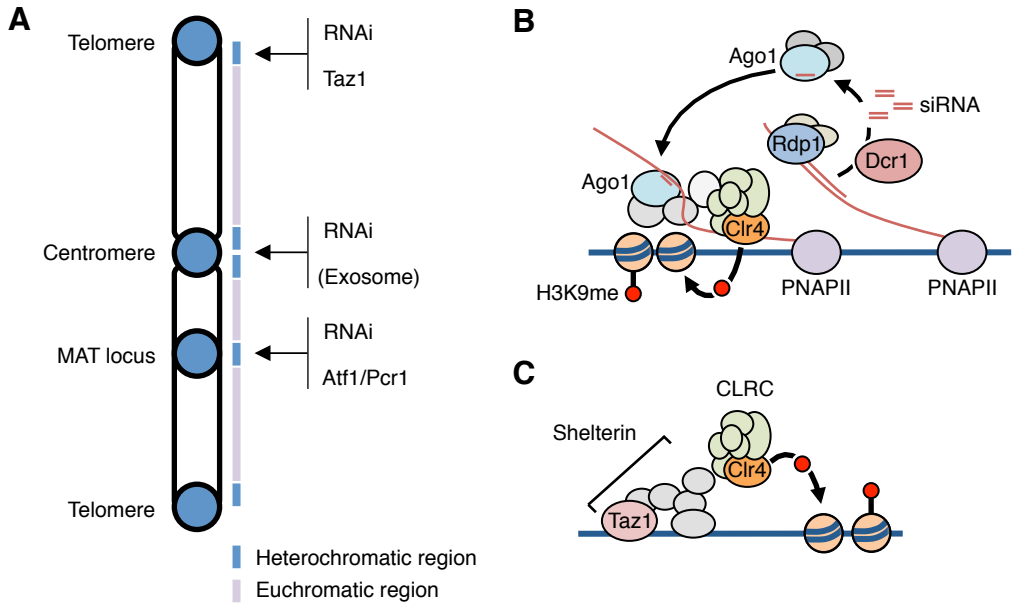

Figure 2. Heterochromatin loci and its assembly pathways in fission yeast

(A) Heterochromatin is formed at centromeres, subtelomeres, and the mating-type (MAT) locus. (B) RNAi-mediated heterochromatin assembly pathway. Dicer processes double-stranded RNA derived from repeat sequence to produce siRNA. The Ago1 protein containing single-stranded siRNA binds to transcripts of the repeat and recruits the CLRC complex. For details, see text. (C) Taz1/Shelterin-mediated heterochromatin assembly pathway. Shelterin, which contains the telomere DNA-binding protein Taz1, recruits the CLRC complex to telomeres to form heterochromatin.

Centromeric heterochromatin formation depends mainly on the RNAi (RNA interference) pathway (Figure 2A and 2B) [12–14]. Centromeres harbor repeat sequences, which are transcribed by PNA polymerase II; transcripts of centromeric repeats are converted to double-stranded RNA by the RNA-directed RNA polymerase Rdp1; and the double-stranded RNA is processed by the endonuclease Dcr1 (Dicer) to develop into siRNA (small interfering RNA) [12, 15–19]. siRNA is bound to Ago1 (Argonaute) to guide the RITS (RNA-induced initiation of transcriptional gene silencing) complex, which contains Ago1, to transcripts of centromeric repeats [20, 21]. RITS interacts with the Clr4-containing protein complex CLRC (Clr4-Rik1-Cul4) to promote methylation of H3K9 at centromeric repeats [22–24]. Clr4 has, in addition to the methyltransferase domain, the chromo domain (CD) to bind to methyl-H3K9, which allows H3K9me to spread along chromatin and maintain the H3K9me level [25]. Exosome-dependent RNA degradation is the second mechanism contributing to

centromeric heterochromatin formation [26–28]. In the presence of exosome, centromeric heterochromatin can be partially established without RNAi machinery [26]. Although the exosome-mediated H3K9me depostion mechanism is not fully understood, RNAi is thought to be the primary pathway to form centromeric heterochromatin.

Subtelomeric heterochromatin assembly relies redundantly on RNAi and the telomere DNA-binding protein Taz1 (Figure 2C) [29]. Taz1 is a component of the telomere protection complex Shelterin, which interacts with Clr4 [30–32]. Subtelomeres harbor a centromeric repeat-like sequence that recruits RNAi machinery. However, this assembly scheme might not be applicable to subtelomeric heterochromatin of chromosome III. The Chromosome III subtelomeres contain ribosomal DNA (rDNA) repeats, which lie adjacent to telomeres and are subject to heterochromatin silencing. However, the assembly mechanism of heterochromatin at rDNA repeats is largely unknown [11, 33–35]. Heterochromatin formation at the mating-type locus depends redundantly on RNAi and ATF/CREB family proteins Atf1/Pcr1 [36]. In addition to centromeric repeat-like sequence, the MAT locus harbors at least two Atf1/Pcr1-binding sites [37]. Atf1 is a transcriptional activation factor, while being thought to promote H3K9me deposition in a different mode, although the Atf1-dependent H3K9me deposition mechanism is still unknown [37, 38].

Heterochromatic marker genes, *ade6* and *ura4*, are commonly used for observation of the silencing state of the inserted region with specific media [39–41]. *ade6* is required for *de novo* inosine monophosphate (IMP) biosynthesis and encodes a carboxylase that converts 5-aminoimidazole ribotide (AIR) to 4-carboxy-5-aminoimidazole ribotide (CAIR). Since AIR develops into a red pigment through multiple steps, Ade6-lacking cells, in which AIR accumulates, form red colonies on an adenine-limited medium. When *ade6* is inserted into a heterochromatin region with endogenous *ade6* disrupted, inserted *ade6* is silenced by heterochromatin, leading to a red phenotype; but in the heterochromatin-deficient strain, inserted *ade6* is expressed to metabolize AIR, leading to a pink or white phenotype. The *ura4* product is involved in the *de novo* uridine monophosphate (UMP) biosynthetic pathway and converts orotidine monophosphate to UMP. Cells lacking *ura4* do not grow on a uracil-lacking medium but are resistant to 5-fluoroorotic acid (5-FOA). 5-FOA is an orotic acid analog converted to 5-FUMP via

two steps with Ura5 and Ura4 activity, which finally develops into the toxic metabolite 5-FdUMP. 5-FdUMP inhibits thymidylate synthase, which converts dUMP to dTMP, thereby inducing depletion of dTTP. The *ura4* marker gene inserted in heterochromatic region visualizes the heterochromatin state with uracil-lacking or 5-FOA-containing medium. Note that because a lot of cellular reactions constitute a marker-associated phenotype, it is possible that perturbation in a reaction step produces a phenotype unrelated to the silencing state of the marker gene.

I-3. Epe1 is a putative demethylase of methyl-H3K9

Epe1 (enhancer of position effect 1) was initially identified as a factor to form the heterochromatin-euchromatin boundary at the mating-type locus [42]. Loss of *epe1* induces heterochromatin spreading with an increase in the H3K9me2 level beyond the natural boundary [42–44]. Overexpression of Epe1 reduced the H3K9me2 level at heterochromatic regions but largely retained the H3K9me3 level [43, 45]. Epe1 physically interacts with a fission yeast HP1 homolog protein, Swi6, and is localized to the constitutive heterochromatin regions (centromeres, subtelomeres, and the mating-type locus) in a largely Swi6-dependent manner [43]. These results suggest that Epe1 counteracts methylation of H3K9 via its interaction with Swi6 (Figure 3). However, the role that Epe1 plays on constitutive heterochromatin is unknown.

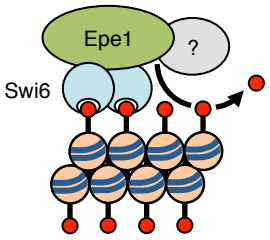

Figure 3. Model of Epe1-mediated demethylation of methyl-H3K9

It is predicted that Epe1 binds to a Swi6 dimer to be localized to heterochromatin and removes H3K9me marks from heterochromatin. It is possible that Epe1 requires another factor for demethylation.

Epe1 is a 108-kDa protein composed of 948 amino acids, and contains the JmjC domain, a conserved domain for demethylation of methyl-lysine of histone proteins (Figure 4). However, its demethylation activity has not been detected by *in vitro* demethylation assay [46]. In this assay, Tsukada et al. employed the mammalian histone methyltransferese G9a to methylate histone H3 up to H3K9me2 [47] and Sf9 cells to obtain recombinant FLAG-tagged Epe1. This suggests that demethylation via Epe1 requires an unidentified mechanism such as interaction with some molecules including another demethylase, post-translational modification of Epe1, and nucleosome formation of the substrate (Figure 3).

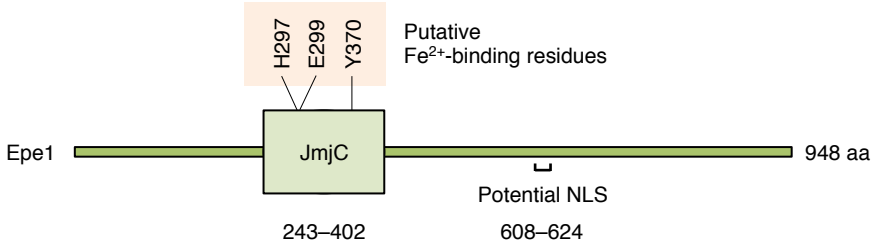

Figure 4. The JmjC domain-containing protein Epe1

Schematic representation of the Epe1 protein. The JmjC domain, putative metal-binding residues, and potential NLS are shown. The JmjC domain is positioned at 243–402 amino acid region as assigned in the SMART database (http://smart.embl-heidelberg.de).

The JmjC domain is conserved from yeast to human, and requires Fe^{2+} and 2-oxoglutarate as cofactors for demethylation reaction [48–50]. The JmjC domain of Epe1 lacks conservation of two of the three residues required for binding to Fe^{2+} [48, 51]. Epe1 bears a substitution of aspartic acid by glutamic acid at the second residue and of histidine by tyrosine at the third one (E299 and Y370 in Figure 4) [46, 48, 51]. It is believed that the latter substitution potentially generates substrate specificity and a requirement for specific conditions for reaction, leading to the difficulty in the detection of the demethylation activity *in vitro* [46, 48, 51]. The histidine-to-tyrosine substitution at the third residue is shared with JmjC domains of mammalian PHF2 and budding yeast Gis1 [48, 51]. In addition, zebra fish phf2 bears the histidine-to-asparagine substitution. Human PHF2 demethylates H3K9me1 but not me2 or me3 *in vivo* [52]. Human PHF2 with the Y-to-H substitution displayed almost the same metal-binding

affinity as wild-type, but neither of them shows demethylation activity *in vitro* [53]. PHF2 phosphorylated by PKA demethylates H3K9me2 *in vitro* [54]. Furthermore, Gis1 displays an increase in *in vitro* demethylation activity toward H3K36me2 in the presence of heme [55]. These findings imply that Epe1 requires specific conditions to display demethylation activity *in vitro*.

H3K9-specific demethylases form the JHDM2 subgroup (also known as KDM3 subgroup) [48]. However, Epe1 is a member of the JHDM1 (KDM2) subgroup composed of H3K36 demethylases, but Epe1 does not demethylate H3K36me [46, 48]. Epe1 may therefore not be a canonical H3K9 demethylase. Gis1 is a member of the JHDM3/JMJD2 subgroup (also known as KDM4 subgroup). PHF2, PHF8, and KIAA1718 proteins form the PHF2/PHF8 subgroup distinguished from the other JmjC subgroups. The H-to-Y substitution at the third metal-binding residue appears across subgroups. Epe1, PHF2, and Gis1 might have uniquely evolved in each subgroup.

Recent studies confirmed the demethylation function of Epe1 *in vivo*. Ragunathan et al. and Audergon et al. established an artificial heterochromatin construction system in fission yeast cells using the TetO sequence combined with the catalytic domain of Clr4 fused to TetR, which binds to TetO but is released by tetracycline treatment of the cells [56, 57]. In the absence of tetracycline, the engineered Clr4 deposits H3K9me at a TetO-integrated locus, and the initial H3K9me is expanded by wild-type Clr4 to develop into heterochromatin. After addition of tetracycline, which induces release of the engineered Clr4, the artificial heterochromatin is retained in the *epe1*Δ background but is depleted in the *epe1*$^{+}$ background. In addition, H3K9me levels are reduced in the presence of Epe1 during cell cycle arrest at G2 phase, which does not induce replication-coupled histone exchange. These suggest that Epe1 promotes active removal of H3K9me independently of the replication-associated passive dilution of old histone.

I-4. Epe1 contributes to formation of stable heterochromatin structure

Loss of *epe1* induces a variegated phenotype through *otr1R::ade6*$^{+}$, an *ade6* marker inserted in a centromeric heterochromatin region; red, pink, and white colonies appear on adenine-limited plate medium [44]. Replating red colonies induces *epe1*Δ-like

variegation, whereas replating white colonies frequently produces white colonies with some red/pink ones. These phenotypes indicate that the centromeric heterochromatin state can be altered in *epe1*Δ cells but the altered state persists to some extent. A similar "plasticity and persistence" phenotype is observed in centrimeric *ura4* markers with 5-FOA [42–44]. However, the mechanism for generating epigenetic variegation in *epe1*Δ cells remains unknown. Moreover, the *epe1*Δ-induced pink and white phenotypes on low adenine plates suggest that the centromeric *ade6* marker is desilenced because of impaired heterochromatin [44]. It is also unknown why the putative H3K9 demethylase Epe1 is involved in stable heterochromatin maintenance.

Loss of Epe1 partially destabilizes centromeric heterochromatin at centromeric marker genes, while loss of a key RNAi factor such as Ago1 and Dcr1 completely disrupts it. Interestingly, *epe1*Δ *ago1*Δ and *epe1*Δ *dcr1*Δ strains show an *epe1*Δ-like variegated phenotype in the *ort1R::ade6*$^{+}$ marker. This indicates that loss of *epe1* suppresses the heterochromatin disruption induced by loss of RNAi, *i.e. epe1*Δ bypasses the requirement for RNAi for heterochromatin maintenance [43, 44, 58]. The mechanism underlying the RNAi bypass remains unknown, although it is predicted that loss of *epe1* enhances the spread of heterochromatin using the residual H3K9me.

I-5. Localization and functions of Epe1 at heterochromatin

Epe1 localizes to nuclear, which is shown by the Epe1-GFP fusion protein [42]. Although a putative nuclear localization signal (NLS) is suggested at positions 608 to 624, the actual NLS is not identified (Figure 4) [42].

Epe1 interacts with the fission yeast HP1 proteins, Swi6 and Chp2 [59], but since loss of Swi6 leads to complete dissociation of Epe1 from constitutive heterochromatin, heterochromatin localization of Epe1 depends mainly on the interaction with Swi6 [43]. Swi6 is phosphorylated by casein kinase II (CK2) and loss of CK2 enhances recruitment of Epe1 to heterochromatin without alteration in H3K9me2 and Swi6 levels, suggesting that CK2-dependent phosphorylation of Swi6 controls Epe1 localization at heterochromatin [60].

Inverted repeat (*IR*) elements are identified as a chromatin boundary sequence lying between heterochromatin and euchromatin regions [61, 62]. Epe1 is enriched in *IR* elements at a higher level than in inner regions of heterochromatin, which is inconsistent with the similar Swi6 or H3K9me2 level at *IR* elements to that at inner regions [43, 63]. *IR* elements flank the left and right sides of the mating-type locus, *cen1*, and *cen3* [11, 62]. The mechanism to form the boundary of *cen2* and subtelomeres is unknown. In the S phase, Epe1 at inner heterochromatin is degraded by proteasome via ubiquitylation by the Cul4-Ddb1^{Cdt2} ubiquitin ligase, which retains Epe1 at chromatin boundaries at a high level [63]. In addition, Epe1 is enriched at a boundary of subtelomeric heterochromatin without *IR* elements [63]. It is likely that Epe1 is enriched not by *IR*-binding factors but by protection of Epe1 at the border of heterochromatic and euchromatic domains. However, how cells limit the accessibility of the Cul4-Ddb1^{Cdt2} complex at boundaries is unknown.

Epe1 is required to restrain outer spreading of constitutive heterochromatin. Like loss of Epe1, mutations in Epe1 at a conserved residue of the JmjC domain allow centromeric heterochromatin to extend outward [43, 44]. Because of lack of the conserved residue in the Epe1 JmjC domain and no *in vitro* evidence for demethylase activity, it is still possible that the boundary formation mechanism does not require the putative histone demethylation function of Epe1 [43, 44]. Epe1 recruits a bromodomain protein, Bdf2, to centromeric boundaries through physical interaction, and antagonizes Sir2-medeiated histone deacetylation that is required for the outer spreading of centromere heterochromatin [64]. Although Epe1 is a well-characterized boundary factor, it is shown that tRNA genes and noncoding RNAs have a boundary formation function [62, 65]. Multiple mechanisms might contribute to boundary formation cooperatively.

Overexpression of Epe1 (Epe1OE) promotes transcription of *ade6* and *ura4* marker genes inserted in centromeric heterochromatin [43, 44]. Intriguingly, this phenotype is also observed in overexpression of JmjC mutants of Epe1, suggesting that Epe1 promotes heterochromatic transcription independently of its potential JmjC-mediated demethylation function [43, 44]. Epe1OE-induced transcriptional activation is based on its physical interaction with SAGA (Spt-Ada-Gcn5 acetyltransferase), a histone

acetyltransferase complex [66]. These raise the possibility that overexpressed Epe1 reduces H3K9me2 levels via a JmjC-independent mechanism [43]. Note that Epe1OE cells largely retain H3K9me3 and Swi6 levels [43]. Thus, increased expression of centromeric marker genes does not necessarily indicate heterochromatin disruption. Epe1 overexpression enhances replacement of histone H3 in heterochromatin, but a requirement for JmjC for histone turnover has not been investigated [67]. The Epe1OE-related observations suggest that Epe1 has multiple activities, and each of them should be separated for understanding of the functions of Epe1.

I-6. Genome-wide functions of Epe1

Genome-wide analysis identifies twenty-one small H3K9me2 peaks designated as heterochromatin islands (*Is*) in euchromatin regions [68]. Loss of Epe1 elevates the H3K9me2 level of several identified islands and induces emergence of additional islands, suggesting that Epe1 counteracts deposition of H3K9 methylation genome-wide [32, 45, 68–70]. Combined loss of Epe1 and the histone acetyltransferase Mst2 induces strong ectopic heterochromatin formation on many euchromatic loci including essential genes, resulting in a severe growth defect [69]. The cell growth can be restored by heterochromatin formation on a heterochromatin assembly gene, *clr4* or *rik1*. Epe1 and Mst2 therefore cooperatively suppress ectopic heterochromatin formation. As described above, Epe1 removes H3K9me deposited in euchromatic regions by the artificial Clr4-tethering system in a JmjC-dependent manner [56, 57]. These studies suggest that Epe1 targets ectopic heterochromatin and antagonizes heterochromatin formation in euchromatic regions via its JmjC-dependent function, although whether Epe1 actually removes H3K9me in spontaneously established ectopic heterochromatin is not known.

Epe1 is localized to several heterochromatin islands related to meiosis in a Swi6-dependent manner and facilitates transcription of meiotic genes when it is overexpressed [43, 70]. Epe1 is also localized to two euchromatic regions in a Swi6-independen manner [43]. In addition, Epe1OE upregulates ten clusters of coding genes [45]. These results suggest existence of an unidentified mechanism by which Epe1 binds to euchromatin, and raise the possibility that Epe1 enhances transcription in euchromatic regions.

I-7. Mechanisms for ectopic heterochromatin formation

Although heterochromatin islands are identified in cells grown in a complete medium, large part of the islands disappears during nitrogen starvation, suggesting that a facultative H3K9me deposition or erasure mechanism exists [68]. Furthermore, a lot of H3K9me deposition sites appear at low temperature [71]. In addition to loss of Epe1 or Mst2, loss of Leo1, a component of the transcription elongation complex Paf1C, enhances genome-wide ectopic H3K9me deposition, and the deposition sites are different among these mutants [68, 69, 72–74]. Methyltransferase activity of Clr4 is intrinsically repressed by auto-methylation of its catalytic site; a mutation that inhibits the auto-methylation makes Clr4 constitutively active, promoting ectopic H3K9me deposition genome-wide [75]. Together, ectopic H3K9me deposition can be induced by specific conditions or genetic modifications, suggesting that there exist many potential mechanisms to deposit H3K9me in euchromatic regions.

Accumulating evidence has uncovered some parts of the mechanisms to deposit ectopic H3K9me. Overlapping transcripts from a convergent gene pair induce deposition of H3K9me3 and Swi6 in the G1 phase through RNAi machinary [76]. Overexpression of Dcr1 promotes processing of double-stranded RNAs into siRNA targeted by RNAi machinary to deposit H3K9me2 at several euchromatic regions [77]. Loss of the exosome catalytic subunit Rrp6 induces RNAi-dependent H3K9me deposition, the regions of which, designated as HOOD (heterochromatin domain), are distinct from islands; transcripts escaped from degradation by Rrp6 are targeted by RNAi [78]. Two heterochromatin islands harbor a meiotic gene that contains DSR (determinant of selective removal) elements [43, 68, 79, 80]. DSR-containing transcripts recruit an RNA-binding protein, Mmi1, which interacts with Clr4, leading to deposition of H3K9me in an RNAi-independent manner [68, 70, 81–83]. Noncoding RNA *ptr* contains DSR elements and is produced in response to phosphate. *ptr* recruits Mmi1 via its DSR to deposit H3K9me2, thereby repressing the *pho1* gene located downstream of *ptr* [84]. The mechanism to silence *pho1* requires RNAi and is enhanced by *rrp6*Δ, which is distinct from that for constructing the DSR-harboring heterochromatin islands. Six out of twenty-one heterochromatin islands harbor both a

late DNA replication origin and several copies of the telomere repeat, where Taz1 recruits Clr4 to deposit H3K9me2 [32]. An increase in stalling of RNA polymerase II by mutation in a transcription elongation factor induces formation of ectopic heterochromatin independently of RNAi, the regions of which are termed pause-induced ectopic heterochromatic region (PIER) [85]. These heterochromatin formation mechanisms potentially make a change in gene expression, which might affect cell growth or allow cells to fit in specific conditions.

I-8. Purpose of this study

Suppression of unscheduled epigenetic alterations is important for maintenance of homogeneity among clonal cells or isogenic individuals, while emergence of epigenetic differences is also important for adaptation or differentiation. The mechanisms that balance both processes warrant further investigation. In this study, I focused on the mechanism for protecting the genome from improper heterochromatin formation in euchromatic regions for constitutive gene expression. I revealed that the JmjC domain-containing protein Epe1 counteracted genome-wide ectopic heterochromatin formation by combination of its JmjC-dependent and JmjC-independent functions. Furthermore, I showed that the counteracting activity of Epe1 is limited in a dose-dependent manner; single copy Epe1 allows some ectopic heterochromatin to persist. Therefore, Epe1 could be a key factor for regulating plasticity and persistence of individual epigenetic profiles.

II. Experimental procedure

II-1. Strains and media for *S. pombe*

The *S. pombe* strains used in this study are listed in Table 1. The media recipes used were previously described [86, 87]. The isolated clones were obtained by two rounds of single-colony isolation, in which "R" or "W" in the strain name means sequential red- or white-colony isolation. The DNA fragments for gene deletion or tagging were constructed using the polymerase chain reaction (PCR)-based method as previously described [88]. For gene deletion, target genes were replaced by the drug-resistant cassettes *kanMX6*, *hphMX6*, and *natMX6* that confer resistance to G418, hygromycin B, and nourseothricin, respectively. The cassettes for expressing 3FLAG-tagged Epe1 and its mutants were constructed on plasmids. The cassettes were then cut out with *Sma*I and introduced into *S. pombe* cells. The 3FLAG tag was placed at the N-terminus of Epe1; C-terminal tagging was avoided because of its effect on Epe1 functions [45, 74]. The four copies of a Taz1 binding sequence (*4TBS*) were represented by 5'-GGGTTACAGGGGTTACAGGGGTTACAGGGGTTACAG-3', composed of four GGTTACAG sequences combined with guanine stretches [89, 90]. For overexpression of 3FLAG-tagged Epe1 (Epe1OE), the *urg1* promoter and *3FLAG* sequence were inserted between the promoter and the CDS of *epe1*. All integrations were confirmed by PCR. The haploid h^+ and h^- strains composing diploid cells harbor *kanMX6* and *natMX6* at the *epe1* locus, respectively. Diploid cell formation was confirmed by dark magenta color on medium containing 5 mg/L Phloxine B (PB; Nacalai Tesque) and resistance to both 100 mg/L G418 sulfate (Wako) and ClonNAT (nourseothricin dihydrogen sulfate; WERNER BioAgents).

Name	Genotype	Epiclone	Source
FY2002	*h⁺ leu1-32 ade6-DN/N ura4-DS/E imr1L(NcoI)::ura4⁺ otr1R(SphI)::ade6⁺*		RC Allshire
FY648	*h⁺ leu1-32 ade6-m210 ura4-DS/E otr1R(SphI)::ura4⁺*		RC Allshire
TP4-1D	*h⁺ leu1-32 ade6-M210 ura4-D18 his2*		M Yanagida
MSS001	*h⁺ leu1-32 ade6-DN/N ura4-DS/E imr1L(NcoI)::ura4⁺ otr1R(SphI)::ade6⁺ epe1Δ::kanMX6*		this study
MSS026	*h⁺ leu1-32 ade6-DN/N ura4-DS/E imr1L(NcoI)::ura4⁺ otr1R(SphI)::ade6⁺ swi6Δ::hphMX6*		this study
MSS069	*h⁺ leu1-32 ade6-DN/N ura4-DS/E imr1L(NcoI)::ura4⁺ otr1R(SphI)::ade6⁺ epe1Δ::kanMX6*	*epe1*Δ R69	this study
MSS070	*h⁺ leu1-32 ade6-DN/N ura4-DS/E imr1L(NcoI)::ura4⁺ otr1R(SphI)::ade6⁺ epe1Δ::kanMX6*	*epe1*Δ W70	this study
MSS075	*h⁺ leu1-32 ade6-DN/N ura4-DS/E imr1L(NcoI)::ura4⁺ otr1R(SphI)::ade6⁺ clr4Δ::natMX6*		this study
MSS103	*h⁺ leu1-32 ade6-DN/N ura4-DS/E imr1L(NcoI)::ura4⁺ otr1R(SphI)::ade6⁺ ago1Δ::hphMX6*		this study
MSS105	*h⁺ leu1-32 ade6-DN/N ura4-DS/E imr1L(NcoI)::ura4⁺ otr1R(SphI)::ade6⁺ epe1Δ::kanMX6 ago1Δ::hphMX6*		this study
MSS147	*h⁺ leu1-32 ade6-m210 ura4-DS/E otr1R(SphI)::ura4⁺ epe1Δ::kanMX6*		this study
MSS148	*h⁺ leu1-32 ade6-m210 ura4-DS/E otr1R(SphI)::ura4⁺ ago1Δ::hphMX6*		this study
MSS164	*h⁺ leu1-32 ade6-DN/N ura4-DS/E imr1L(NcoI)::ura4⁺ otr1R(SphI)::ade6⁺ epe1Δ::kanMX6*	*epe1*Δ W164	this study
MSS165	*h⁺ leu1-32 ade6-DN/N ura4-DS/E imr1L(NcoI)::ura4⁺ otr1R(SphI)::ade6⁺ epe1Δ::kanMX6*	*epe1*Δ W165	this study
MSS166	*h⁺ leu1-32 ade6-DN/N ura4-DS/E imr1L(NcoI)::ura4⁺ otr1R(SphI)::ade6⁺ epe1Δ::kanMX6*	*epe1*Δ W166	this study
MSS173	*h⁹⁰ leu1-32 ade6-DN/N ura4-DS/E imr1L(NcoI)::ura4⁺ otr1R(SphI)::ade6⁺ epe1Δ::kanMX6 ago1Δ::hphMX6*	*epe1*Δ *ago1*Δ W173	this study
MSS185	*h⁺ leu1-32 ade6-DN/N ura4-DS/E imr1L(NcoI)::ura4⁺ otr1R(SphI)::ade6⁺ ade5Δ::hphMX6*		this study
MSS188	*h⁺ leu1-32 ade6-m210 ura4-DS/E otr1R(SphI)::ura4⁺ ade5Δ::hphMX6*		this study
MSS190	*h⁺ leu1-32 ade6-m210 ura4-DS/E otr1R(SphI)::ura4⁺ clr4Δ::natMX6*		this study
MSS192	*h⁺ leu1-32 ade6-m210 ura4-DS/E otr1R(SphI)::ura4⁺ epe1Δ::kanMX6 ago1Δ::hphMX6*		this study
MSS220	*h⁺ leu1-32 ade6-m210 ura4-DS/E otr1R(SphI)::ura4⁺ clr3Δ::hphMX6*		this study
MSS222	*h⁺ leu1-32 ade6-m210 ura4-DS/E otr1R(SphI)::ura4⁺ epe1Δ::kanMX6 clr3Δ::hphMX6*		this study
MSS224	*h⁺ leu1-32 ade6-m210 ura4-DS/E otr1R(SphI)::ura4⁺ epe1Δ::kanMX6 clr4Δ::natMX6*		this study
MSS242	*h⁺ leu1-32 ade6-m210 ura4-DS/E otr1R(SphI)::ura4⁺ sir2Δ::natMX6*		this study
MSS250	*h⁺ leu1-32 ade6-m210 ura4-DS/E otr1R(SphI)::ura4⁺ epe1Δ::kanMX6 sir2Δ::natMX6*		this study
MSS271	*h⁺ leu1-32 ade6-DN/N ura4-DS/E imr1L(NcoI)::ura4⁺ otr1R(SphI)::ade6⁺ gal1Δ::natMX6*		this study
MSS279	*h⁺ leu1-32 ade6-m210 ura4-DS/E otr1R(SphI)::ura4⁺ taz1Δ::natMX6*		this study
MSS290	*h⁺ leu1-32 ade6-m210 ura4-DS/E otr1R(SphI)::ura4⁺ epe1Δ::kanMX6 taz1Δ::natMX6*		this study
MSS309	*h⁺ leu1-32 ade6-m210 ura4-DS/E otr1R(SphI)::ura4⁺ swi6Δ::hphMX6*		this study
MSS311	*h⁺ leu1-32 ade6-m210 ura4-DS/E otr1R(SphI)::ura4⁺ epe1Δ::kanMX6 swi6Δ::hphMX6*		this study
MSS332	*h⁺/h⁻ leu1-32/leu1⁺ ade6-DN/N/ade6-DN/N ura4-DS/E/ura4-DS/E imr1L(NcoI)::ura4⁺/imr1L(NcoI)::ura4⁺ otr1R(SphI)::ade6⁺/otr1R(SphI)::ade6⁺ epe1Δ::kanMX6/epe1Δ::natMX6*	derived from *epe1*Δ W70	this study
MSS335	*h⁺/h⁻ leu1-32/leu1⁺ ade6-DN/N/ade6-DN/N ura4-DS/E/ura4-DS/E imr1L(NcoI)::ura4⁺/imr1L(NcoI)::ura4⁺ otr1R(SphI)::ade6⁺/otr1R(SphI)::ade6⁺ epe1Δ::kanMX6/epe1Δ::natMX6 ade5⁺/ade5Δ::hphMX6*	derived from *epe1*Δ W70	this study
MSS354	*h⁺/h⁻ leu1-32/leu1⁺ ade6-DN/N/ade6-DN/N ura4-DS/E/ura4-DS/E imr1L(NcoI)::ura4⁺/imr1L(NcoI)::ura4⁺ otr1R(SphI)::ade6⁺/otr1R(SphI)::ade6⁺ epe1Δ::kanMX6/epe1⁺::natMX6*	derived from *epe1*Δ W70	this study
MSS358	*h⁺/h⁻ leu1-32/leu1⁺ ade6-DN/N/ade6-DN/N ura4-DS/E/ura4-DS/E imr1L(NcoI)::ura4⁺/imr1L(NcoI)::ura4⁺ otr1R(SphI)::ade6⁺/otr1R(SphI)::ade6⁺ epe1Δ::kanMX6/epe1⁺::natMX6 ade5⁺/ade5Δ::hphMX6*	derived from *epe1*Δ W70	this study
MSS365	*h⁺ leu1-32 ade6-m210 ura4-DS/E otr1R(SphI)::ura4⁺ epe1Δ::kanMX6 ago1Δ::hphMX6 taz1Δ::natMX6*		this study
MSS367	*h⁺/h⁻ leu1-32/leu1⁺ ade6-DN/N/ade6-DN/N ura4-DS/E/ura4-DS/E imr1L(NcoI)::ura4⁺/imr1L(NcoI)::ura4⁺ otr1R(SphI)::ade6⁺/otr1R(SphI)::ade6⁺ epe1Δ::kanMX6/epe1⁺::natMX6*		this study
MSS371	*h⁻ leu1-32 ade6-m210 ura4-DS/E otr1R(SphI)::ura4⁺ ago1Δ::hphMX6 taz1Δ::natMX6*		this study
MSS378	*h⁺/h⁻ leu1-32/leu1⁺ ade6-DN/N/ade6-DN/N ura4-DS/E/ura4-DS/E imr1L(NcoI)::ura4⁺/imr1L(NcoI)::ura4⁺ otr1R(SphI)::ade6⁺/otr1R(SphI)::ade6⁺ epe1⁺::kanMX6/epe1⁺::natMX6*		this study
MSS415	*h⁺/h⁻ leu1-32/leu1⁺ ade6-DN/N/ade6-DN/N ura4-DS/E/ura4-DS/E imr1L(NcoI)::ura4⁺/imr1L(NcoI)::ura4⁺ otr1R(SphI)::ade6⁺/otr1R(SphI)::ade6⁺ epe1Δ::kanMX6/epe1Δ::natMX6*		this study
MSS417	*h⁺/h⁻ leu1-32/leu1⁺ ade6-DN/N/ade6-DN/N ura4-DS/E/ura4-DS/E imr1L(NcoI)::ura4⁺/imr1L(NcoI)::ura4⁺ otr1R(SphI)::ade6⁺/otr1R(SphI)::ade6⁺ epe1Δ::kanMX6/epe1Δ::natMX6 ade5⁺/ade5Δ::hphMX6*		this study
MSS419	*h⁺/h⁻, leu1-32/leu1⁺, ade6-DN/N/ade6-DN/N, ura4-DS/E/ura4-DS/E, imr1L(NcoI)::ura4⁺/imr1L(NcoI)::ura4⁺, otr1R(SphI)::ade6⁺/otr1R(SphI)::ade6⁺, epe1Δ::kanMX6/epe1⁺::natMX6, ade5⁺/ade5Δ::hphMX6*		this study

Name	Genotype	Epiclone	Source
MSS422	*h⁺/h⁻ leu1-32/leu1⁺ ade6-DN/N/ade6-DN/N ura4-DS/E/ura4-DS/E imr1L(NcoI)::ura4⁺/imr1L(NcoI)::ura4⁺ otr1R(SphI)::ade6⁺/otr1R(SphI)::ade6⁻ epe1⁺::kanMX6/epe1⁺::natMX6 ade5⁺/ade5Δ::hphMX6*		this study
MSS424	*h⁺/h⁻ leu1-32/leu1⁺ ade6-DN/N/ade6-DN/N ura4-DS/E/ura4-DS/E imr1L(NcoI)::ura4⁺/imr1L(NcoI)::ura4⁺ otr1R(SphI)::ade6⁺/otr1R(SphI)::ade6⁻ epe1⁺::kanMX6/epe1⁺::natMX6 ade5Δ::hphMX6/ade5Δ::hphMX6*		this study
MSS452	*h⁻ leu1-32 ade6-m210 ura4-DS/E otr1R(SphI)::ura4⁺*		this study
MSS454	*h⁻ leu1-32 ade6-m210 ura4-DS/E otr1R(SphI)::ura4⁺ epe1Δ::natMX6*		this study
MSS464	*h⁻ leu1-32 ade6-m210 ura4-DS/E otr1R(SphI)::ura4⁺ epe1Δ::natMX6 SPCC569.06Δ::LEU2*		this study
MSS470	*h⁻ leu1-32 ade6-m210 ura4-DS/E otr1R(SphI)::ura4⁺ epe1Δ::natMX6 SPCC569.06Δ::LEU2-4TBS*		this study
MSS473	*h⁺ leu1-32 ade6-m210 ura4-DS/E otr1R(SphI)::ura4⁺ kanMX6-Purg1-3×FLAG-epe1*		this study
MSS503	*h⁻ leu1-32 ade6-m210 ura4-DS/E otr1R(SphI)::ura4⁺ epe1Δ::natMX6*	*epe1*Δ W-t1	this study
MSS504	*h⁺/h⁻ leu1-32/leu1-32 ade6-m210/ade6-m210 ura4-DS/E/ura4-DS/E otr1R(SphI)::ura4⁺/otr1R(SphI)::ura4⁺ 3×FLAG-epe1::kanMX6/epe1Δ::natMX6 ade5Δ::hphMX6/ade5⁻*	derived from *epe1*Δ W-t1	this study
MSS506	*h⁺/h⁻ leu1-32/leu1-32 ade6-m210/ade6-m210 ura4-DS/E/ura4-DS/E otr1R(SphI)::ura4⁺/otr1R(SphI)::ura4⁺ 3×FLAG-epe1H297A::kanMX6/epe1Δ::natMX6 ade5Δ::hphMX6/ade5⁻*	derived from *epe1*Δ W-t1	this study
MSS513	*h⁺/h⁻ leu1-32/leu1-32 ade6-m210/ade6-m210 ura4-DS/E/ura4-DS/E otr1R(SphI)::ura4⁺/otr1R(SphI)::ura4⁺ kanMX6-Purg1-3×FLAG-epe1/epe1Δ::natMX6 ade5Δ::hphMX6/ade5⁻*	derived from *epe1*Δ W-t1	this study
MSS515	*h⁻ leu1-32 ade6-m210 ura4-DS/E otr1R(SphI)::ura4⁺ epe1Δ::natMX6 SPCC569.06Δ::LEU2-4TBS*	*epe1*Δ *LEU2^{4TBS}* W1-1	this study
MSS517	*h⁺/h⁻ leu1-32/leu1-32 ade6-m210/ade6-m210 ura4-DS/E/ura4-DS/E otr1R(SphI)::ura4⁺/otr1R(SphI)::ura4⁺ 3×FLAG-epe1::kanMX6/epe1Δ::natMX6 ade5Δ::hphMX6/ade5⁺ SPCC569.06⁺/SPCC569.06Δ::LUE2-4TBS*	derived from *epe1*Δ *LEU2^{4TBS}* W1-1	this study
MSS521	*h⁺/h⁻ leu1-32/leu1-32 ade6-m210/ade6-m210 ura4-DS/E/ura4-DS/E otr1R(SphI)::ura4⁺/otr1R(SphI)::ura4⁺ 3×FLAG-epe1H297A::kanMX6/epe1Δ::natMX6 ade5Δ::hphMX6/ade5⁺ SPCC569.06⁺/SPCC569.06Δ::LUE2-4TBS*	derived from *epe1*Δ *LEU2^{4TBS}* W1-1	this study
MSS529	*h⁺/h⁻ leu1-32/leu1-32 ade6-m210/ade6-m210 ura4-DS/E/ura4-DS/E otr1R(SphI)::ura4⁺/otr1R(SphI)::ura4⁺ kanMX6-Purg1-3×FLAG-epe1/epe1Δ::natMX6 ade5Δ::hphMX6/ade5⁺ SPCC569.06⁺/SPCC569.06Δ::LUE2-4TBS*	derived from *epe1*Δ *LEU2^{4TBS}* W1-1	this study
MSS532	*h⁺/h⁻ leu1-32/leu1-32 ade6-m210/ade6-m210 ura4-DS/E/ura4-DS/E otr1R(SphI)::ura4⁺/otr1R(SphI)::ura4⁺ epe1Δ::kanMX6/epe1Δ::natMX6 SPCC569.06⁺/SPCC569.06Δ::LUE2-4TBS*	derived from *epe1*Δ *LEU2^{4TBS}* W1-1	this study
MSS533	*h⁺/h⁻ leu1-32/leu1-32 ade6-m210/ade6-m210 ura4-DS/E/ura4-DS/E otr1R(SphI)::ura4⁺/otr1R(SphI)::ura4⁺ epe1Δ::kanMX6/epe1Δ::natMX6 ade5Δ::hphMX6/ade5⁺ SPCC569.06⁺/SPCC569.06Δ::LUE2-4TBS*	derived from *epe1*Δ *LEU2^{4TBS}* W1-1	this study
MSS550	*h⁺/h⁻ leu1-32/leu1-32 ade6-m210/ade6-m210 ura4-DS/E/ura4-DS/E otr1R(SphI)::ura4⁺/otr1R(SphI)::ura4⁺ 3×FLAG-epe1::kanMX6/epe1Δ::natMX6 ade5Δ::hphMX6/ade5⁺ SPCC569.06⁺/SPCC569.06Δ::LUE2*		this study
MSS558	*h⁺/h⁻ leu1-32/leu1-32 ade6-m210/ade6-m210 ura4-DS/E/ura4-DS/E otr1R(SphI)::ura4⁺/otr1R(SphI)::ura4⁺ epe1Δ::kanMX6/epe1Δ::natMX6*	derived from *epe1*Δ W-t1	this study
MSS562	*h⁺/h⁻ leu1-32/leu1-32 ade6-m210/ade6-m210 ura4-DS/E/ura4-DS/E otr1R(SphI)::ura4⁺/otr1R(SphI)::ura4⁺ epe1Δ::kanMX6/epe1Δ::natMX6 ade5Δ::hphMX6/ade5⁻*	derived from *epe1*Δ W-t1	this study
MSS599	*h⁺/h⁻ leu1-32/leu1-32 ade6-m210/ade6-m210 ura4-DS/E/ura4-DS/E otr1R(SphI)::ura4⁺/otr1R(SphI)::ura4⁺ 3×FLAG-epe1::kanMX6/epe1Δ::natMX6 ade5Δ::hphMX6/ade5⁻*		this study
MSS623	*h⁻ leu1-32 ade6-m210 ura4-DS/E otr1R(SphI)::ura4⁺ 3×FLAG-epe1::kanMX6*		this study
MSS624	*h⁻ leu1-32 ade6-m210 ura4-DS/E otr1R(SphI)::ura4⁺ 3×FLAG-epe1H297A::kanMX6*		this study
MSS650	*h⁻ leu1-32 ade6-m210 ura4-DS/E otr1R(SphI)::ura4⁺ SPCC569.06Δ::LEU2*		this study
MSS705	*h⁺ leu1-32 ade6-m210 ura4-DS/E otr1R(SphI)::ura4⁺ bdf2Δ::natMX6*		this study
MSS767	*h⁻ leu1-32 ade6-m210 ura4-DS/E otr1R(SphI)::ura4⁺ epe1Δ::kanMX6*	*epe1*Δ R1-1	this study
MSS768	*h⁺ leu1-32 ade6-m210 ura4-DS/E otr1R(SphI)::ura4⁺ epe1Δ::kanMX6*	*epe1*Δ R2-1	this study
MSS769	*h⁻ leu1-32 ade6-m210 ura4-DS/E otr1R(SphI)::ura4⁺ epe1Δ::kanMX6*	*epe1*Δ R3-1	this study
MSS770	*h⁺ leu1-32 ade6-m210 ura4-DS/E otr1R(SphI)::ura4⁺ epe1Δ::kanMX6*	*epe1*Δ W1-1	this study
MSS771	*h⁻ leu1-32 ade6-m210 ura4-DS/E otr1R(SphI)::ura4⁺ epe1Δ::kanMX6*	*epe1*Δ W2-1	this study
MSS772	*h⁺ leu1-32 ade6-m210 ura4-DS/E otr1R(SphI)::ura4⁺ epe1Δ::kanMX6*	*epe1*Δ W5-1	this study
MSS773	*h⁻ leu1-32 ade6-m210 ura4-DS/E otr1R(SphI)::ura4⁺ epe1Δ::kanMX6*	*epe1*Δ W6-1	this study
MSS774	*h⁻ leu1-32 ade6-m210 ura4-DS/E otr1R(SphI)::ura4⁺ epe1Δ::kanMX6*	*epe1*Δ W8-1	this study
MSS775	*h⁺ leu1-32 ade6-m210 ura4-DS/E otr1R(SphI)::ura4⁺ epe1Δ::kanMX6*	*epe1*Δ W9-1	this study
MSS781	*h⁻ leu1-32 ade6-m210 ura4-DS/E otr1R(SphI)::ura4⁺ 3×FLAG-epe1H297A::kanMX6*	*epe1H297A* W2-1	this study
MSS795	*h⁺ leu1-32 ade6-m210 ura4-DS/E otr1R(SphI)::ura4⁺ epe1Δ::kanMX6 ago1Δ::hphMX6*	*epe1*Δ *ago1*Δ R1-1	this study
MSS796	*h⁻ leu1-32 ade6-m210 ura4-DS/E otr1R(SphI)::ura4⁺ epe1Δ::kanMX6 ago1Δ::hphMX6*	*epe1*Δ *ago1*Δ R2-1	this study
MSS797	*h⁺ leu1-32 ade6-m210 ura4-DS/E otr1R(SphI)::ura4⁺ epe1Δ::kanMX6 ago1Δ::hphMX6*	*epe1*Δ *ago1*Δ W2-1	this study
MSS798	*h⁻ leu1-32 ade6-m210 ura4-DS/E otr1R(SphI)::ura4⁺ epe1Δ::kanMX6 ago1Δ::hphMX6*	*epe1*Δ *ago1*Δ W4-1	this study
MSS805	*h⁻ leu1-32 ade6-m210 ura4-DS/E otr1R(SphI)::ura4⁺ epe1Δ::kanMX6 taz1Δ::natMX6*	*epe1*Δ *taz1*Δ W7-2	this study

Table 1. Fission yeast strains used in this study

Genotypes of fission yeast strains are shown.

II-2. Serial dilution assay

Saturated cells were adjusted to 1×10^8 cells/mL in sterilized water. For preculture of diploid cells, medium containing 100 mg/L G418 sulfate and ClonNAT was used. Diploid cells were saturated without the antibiotics. The suspended cells were serially 10-fold diluted up to 1×10^3 cells/mL. The suspension (6 or 8 μL) was spotted on YE-based complete media or PMG-based synthetic media. To complement genetic

mutations, supplements mix (225 mg/L adenine, uracil, histidine, leucine, and lysine, as final concentration) was added (YES and PMGS). Silencing assays were performed on YE media with adenine-dropout supplements mix (Low Ade) and PMG media with leucine-dropout supplements mix (–Leu). The galactose-containing medium (YEGal) was made by replacement of the major carbon source: 30 g/L of galactose, instead of glucose, was added to YES. For haploid cells, plates were incubated at 30°C for 4 days. For diploid cells, plates were incubated at 30°C for 3 days. No assay medium contained antibiotics.

II-3. qRT-PCR analysis

Cells were cultured in 20 mL of YES to 1 (within ±0.1) × 10^7 cells/mL. The harvested cells were washed with PBS and stored at −80°C. The cell pellet was suspended in AE buffer (50 mM sodium acetate (pH 5.2) and 10 mM EDTA) containing 1% SDS, and then the equivalent volume of acid phenol was added to the suspension. Total RNA was extracted by a freeze-thaw treatment made up of five cycles of rapid freezing in liquid nitrogen followed by incubation in a water bath at 65°C with vortexing. The RNA was subjected to another acid phenol treatment followed by acid phenol/chloroform and chloroform treatments. RNA was recovered by ethanol precipitation and treated with 5 U of recombinant DNase I (Takara Bio) at 37°C for 30 min. DNase I was removed by acid phenol/chloroform treatment. Using Oligo $(dT)_{15}$ primer, 1 μg of total RNA was reverse transcribed into cDNA with PrimeScript Reverse Transcriptase (Takara Bio) at 37°C for 30 min. Quantitative PCR (qPCR) was performed with SYBR Green I dye on a Thermal Cycler Dice Real Time System TP-850 (Takara Bio). The RT− samples (pseudo-experiments without reverse transcriptase) were also subjected to qPCR. The primer sets are listed in Table 2. The standard curve for each primer set was created from serially 1-to-1000-fold diluted cDNA samples of *clr4*Δ cells. The signals of RT− samples were low and seldom fell within the standard curve, and consequently no RT− sample was adequately analyzed. Relative concentrations of cDNA based on the standard curve were divided by the concentration of *act1* to determine the transcript levels relative to *act1*. The error bars represent the standard deviation of the mean of three independent experiments (n = 3). Each experiment was independently performed from cell culture to qPCR. Note that *ade6-DN/N* harbors a 153 bp of deletion between *Nco*I sites [41]. The primer set for

ade6 specifically detects the centromere-derived transcripts, avoiding amplification of the truncated allele.

ID	Name	Sequence
BP13	*act1* Fw	TGCCGATCGTATGCAAAAGG
BP14	*act1* Rv	CCGCTCTCATCATACTCTTG
BP26	*ade5* Fw	GATGCTACGCTGAATGGAGT
BP27	*ade5* Rv	GCAAAGACGTTGGTATCCCA
BP28	*dg* Fw	CTGCGGTTCACCCTTAACATC
BP29	*dg* Rv	CAACTGCGGATGGAAAAAGT
BP30	*ade6* Fw	GTAGTACGCAGTTTAGACGG
BP31	*ade6* Rv	GAGCACGCTGTTGAATTGAG
SP192	*SPCC569.03* Fw	CGTTCTTGCAAGTCGATGATG
SP193	*SPCC569.03* Rv	CAAGCGGTGGGAGTTCATAG
SP214	*ade1* Fw	GTCAAGGGCTGTAAGCAAGC
SP215	*ade1* Rv	GGAGACAGCTCCAACTGAGG
SP413	*LEU2* Fw	TCGTTCCAATGTCAAGTTCG
SP414	*LEU2* Rv	CCATTTAGGACCACCCACAG
SP421	*gal1* Fw	GTGGTGGAAATGGCAGTTG
SP420	*gal1* Rv	AATGCGGCTGTTTTAGGTG
SP431	*puf6* Fw	CCAGAGCAGGATAACCACTTG
SP432	*puf6* Rv	CTTGTTTCTCAGCACCACTCC
SP433	*nsa2* Fw	CCTCAAAGCCCGACTTATACC
SP434	*nsa2* Rv	ACCACCAGATGTGACAAGACC
SP439	*IRC3* Fw	ATCTTTGGAACGCTCTTACCC
SP440	*IRC3* Rv	GAAAAACTGTGTGAGGCAACC
SP441	*can1* Fw	GGTGGCAGGAAGAAAAGAAAAG
SP442	*can1* Rv	TACGACGTGGAAAACGAATAGG
SP449	*pdi4* Fw	ATTACACCCCGTGAGTTTCG
SP450	*pdi4* Rv	CAGACTGTGGCATTTTGTCG
SP475	*ypt7* Fw	CAACCATAGGAGCGGATTTTC
SP476	*ypt7* Rv	ATAAAACGCAACCCCCAAAC

Table 2. qPCR primers used in this study

The primers used in qRT-PCR and ChIP-qPCR analyses are listed.

II-4. Microarray analysis

The microarray analysis was performed as described previously [91]. Based on the expression ratio, genes with a fold change >1.5 (upregulated) or <1.5 (downregulated) are highlighted. This experiment was not repeated. The sequences of the probes and the original data from the microarray experiments were deposited in GEO (http://www.ncbi.nlm.nih.gov/geo) under accession number GSE108448.

II-5. ChIP-qPCR analysis

Cells grown to 1 (within ±0.1) × 10^7 cells/mL in 50 mL of YES were fixed with 1% formaldehyde (Nacalai Tesque) for 20 min at 25°C. Diploid cells were precultured in YES containing 100 mg/L G418 sulfate and ClonNAT and then grown to 5 (within ±0.5) × 10^6 cells/mL in 50 mL of YES without antibiotics followed by the same formaldehyde treatment as for haploid cells. Quenching of the fixative was performed

with 150 mM glycine. The cells were harvested by centrifugation and stored at −80°C. Note that the diploid cells were stored for no more than 1 day. The cells were resuspended in Buffer 1 (50 mM HEPES-KOH (pH 7.5), 140 mM NaCl, 1mM EDTA, 1% Triton X-100 (Nacalai Tesque), and 0.1% sodium deoxycholate (Merck Millipore)) containing a protease inhibitor cocktail, and then homogenized with 30–40 cycles of bead beating for 60 s at 4°C to render them refraction-negative under a light microscope. The cell extracts were centrifuged for 60 min at 21,880 × *g* at 4°C. After discarding the supernatant, the pellets were resuspended in Buffer 1 containing a protease inhibitor cocktail and sonicated with resonant metallic bars for 360 s with Bioruptor UCW-310 (Cosmo Bio) set at 310 W (High level) and cooled to around 4°C. The sonicated cell extracts were centrifuged for 15 min at 21,880 × *g* at 4°C, and the resultant supernatant was recovered. Before IP, Dynabeads M-280 Sheep anti-Mouse or anti-Rabbit IgG (Invitrogen) were washed once with Buffer 1 and incubated with 1 μg of anti-H3K9me (mouse monoclonal, m5.1.1, a kind gift from T. Urano, Shimane University), anti-FLAG (mouse monoclonal, M2, Sigma-Aldrich), anti-Swi6 (rabbit polyclonal, made by Shinya Takahata, Hokkaido University), anti-H3K9me2 (mouse monoclonal, 6D11, a kind gift from H. Kimura, Tokyo Institute of Technology), or anti-H3K9me3 (mouse monoclonal, 2F3, a kind gift from H. Kimura, Tokyo Institute of Technology) [92] antibody for 2 h with mild rotation at 4°C followed by washing with Buffer 1. Note that the anti-H3K9me antibody detects mono-, di-, and tri-methylated H3K9 but not unmethylated H3K9. The beads were incubated with the supernatant for 2 h with mild rotation at 4°C. After IP, the beads were washed twice each with Buffer 1, Buffer 1' (50 mM HEPES-KOH (pH 7.5), 500 mM NaCl, 1 mM EDTA, 1% Triton X-100, and 0.1% sodium deoxycholate), and Buffer 2 (10 mM Tris-HCl (pH 8.0), 250 mM LiCl, 0.5% NP-40 (Roche), and 0.5% sodium deoxycholate) followed by another wash with Buffer 1. The beads were resuspended in Buffer 1 containing RNase A and incubated for 15 min at 37°C and then incubated in 0.25 mg/mL Proteinase K and 0.25% SDS for 2 h at 37°C to obtain IP samples. For input samples, one-fifth volume of the supernatant applied to IP was equally subjected to RNase A and Proteinase K treatments. IP and input samples were incubated for 12–16 h at 65°C for reverse crosslinking. DNA was extracted by neutral phenol/chloroform treatment and recovered by ethanol precipitation. qPCR was performed with SYBR Green I dye on Thermal Cycler Dice Real Time System TP-850 (Takara Bio). The primer sets are listed in Table 2. The standard curve

for each primer set was created from serially diluted input samples of WT cells. Relative concentrations of IP samples based on the standard curve were divided by those of input samples to determine the IP efficiency (IP/input). For FLAG ChIP analysis, IP efficiency of FLAG-tagged cells was divided by that of no tag (WT) cells to determine fold enrichment (fold over no tag). For Swi6 ChIP analysis, incubation at 18°C for 2 h before fixation, which has been usually done to increase signal intensity in previous studies, was not carried out because low temperature induces ectopic heterochromatin formation [71, 93]. This might have increased background levels. The error bars represent the standard deviation of the mean of three independent experiments (n = 3). Each experiment was independently performed from cell culture to qPCR. The sequencing data of ChIP-seq analyses including input and IP were deposited in DDBJ (http://www.ddbj.nig.ac.jp) under accession number DRA006424 for the *ade6-m210* strains and DRA006425 for the *otr1R::ade6*$^{+}$-harboring strains.

II-6. ChIP-sequencing analysis

Cells were grown to 1 (within ±0.1) × 10^7 cells/mL in 500 mL of YES. The following procedure was identical to that of ChIP-qPCR analysis except for qPCR. In the ChIP-seq analysis of *ade6-m210* cells, DNA was recovered using the spin column-based QIAquick PCR Purification Kit (Qiagen) instead of ethanol precipitation. The ChIP libraries for the Illumina platform were prepared according to the manufacturer's instructions. The libraries from *ade6-m210* and *otr1R::ade6*$^{+}$ strains were sequenced on the Illumina HiSeq 1500 system (single-end, 51 bp) and the HiSeq 2500 system (single-end, 101 bp), respectively. The sequenced reads were mapped onto the *S. pombe* genome (972) using BWA (version 0.7.17), and then processed using SAMtools (version 1.6) and MACS (version 2.1.1). MACS extended each read to the expected fragment length of 200 bp using the option --extsize 200. The processed ChIP-seq data were loaded into IGV. Blue graphs indicate normalized piled-up fragment counts at single base-pair resolution: the scale of the vertical axis is represented as fragment counts per five million mapped reads. The experiments were not repeated.

II-7. Western blotting analysis

Cells grown to 1 × 10^7 cells/mL in 15 mL of YES were harvested, washed, resuspended in water, and heated at 95°C for 5 min. An equal volume of buffer containing 8 M Urea, 4% SDS, 0.12 M Tris-HCl (pH 6.8), 20% glycerol, and 0.6 M β-mercaptoethanol was added to cell suspensions, and the cells were homogenized by bead beating. The cell extracts were heated at 95°C for 5 min and spun down, and then the supernatants were recovered. The supernatant samples were separated by polyacrylamide gel electrophoresis, and the proteins were blotted onto nitrocellulose membranes. The membranes were first probed with the anti-FLAG (M2, Sigma-Aldrich) and anti-α-tubulin (B-5-1-2, Sigma-Aldrich) antibodies, and then with horseradish peroxidase-conjugated anti-Mouse IgG (GE Healthcare).

II-8. Yeast two-hybrid assay

Matchmaker GAL4 Two-Hybrid System 3 (Clontech) was used for the Epe1-Swi6 interaction analysis. pGBKT7 (containing *TRP1*) was used for bait expression. pGADT7 (containing *LEU2*) was used for prey expression. pGBKT7 and pGADT7 plasmids were introduced into the AH109 host strain by a polyethylene glycol/lithium acetate (PEG/LiAc)-mediated method. AH109 harbors a *HIS3* reporter gene. Yeast strains were cultured on proper minimal synthetic dropout (SD) media according to the user manual (Clontech). Glucose was applied to SD media as the carbon source. The experimental procedure for serial dilution assays of *S. cerevisiae* strains was the same as for *S. pombe* strains.

II-9. Colony color assessment

Six hundred cells were spread onto a plate with a 90 mm diameter containing adenine-limited media, which generated 200–500 colonies depending on the mutation. For cell spreading, sterile glass beads were used. The cells were incubated at 30°C for 4 days on adenine-limited media, and photographed for assessment. No image processing software was applied to the assessment. Colony color on adenine-limited medium was assessed in randomized photographs and the sample names were masked. The color was grouped into five types: red or dark red; pale red; reddish pink or pink; light pink; and completely white color. The group “completely white” only included the white color observed in *ade5*Δ cells. Colonies too small for color assessment were grouped into

“too small” and excluded from the percentage graph. Although the color of small colonies appeared pale, colony color was not adjusted for colony size in the assessment. When samples displayed a uniform color (at least >99%), the assessment area was reduced to half of the plate.

II-10. Co-immunoprecipitation analysis

Co-immunoprecipitation analysis was performed as described previously with some modifications [43, 64]. Cells grown to 1 (within ±0.1) × 10^7 cells/mL in 50 mL of YES were harvested by centrifugation, washed with 2 × HC buffer (200 mM HEPES-KOH (pH 7.5), 300 mM KCl, 2 mM EDTA, and 20% glycerol), frozen in liquid nitrogen, and stored at −80°C. Cells were resuspended in 2 × HC buffer containing a protease inhibitor cocktail and 2 mM DTT, and then homogenized with 16 cycles of bead beating for 15 s at 4°C to render 90% of them refraction-negative under a light microscope. The cell lysate was centrifuged for 10 min at 14,000 × *g* at 4°C, and the resultant supernatant was recovered. Twenty microliter of the supernatant was mixed with an equal volume of 2 × Laemmli buffer (8 M Urea, 2% SDS, 0.12 M Tris-HCl (pH 6.8), 20% glycerol, and 0.6 M β-mercaptoethanol) and heated at 95ºC for 5 min. Before IP, Dynabeads M-280 Sheep anti-Mouse IgG (Invitrogen) were washed once with 1 × HC buffer and incubated with 1 μg of anti-FLAG (mouse monoclonal, M2, Sigma-Aldrich) antibody for 2 h with mild rotation at 4°C followed by washing with 1 × HC buffer. The beads were suspended in the cell lysate mixed with an equal volume of 200 mM KCl containing a protease inhibitor cocktail, and incubated for 4 h with mild rotation at 4°C, where IP reaction was actually performed in 1 × HC buffer containing 250 mM KCl and 1 mM DTT. After IP, the beads were washed eight times with 1 × HC buffer containing 250 mM KCl, suspended in 20 μl of 1 × HC buffer followed by addition of an equal volume of 2 × Laemmli buffer, heated at 95ºC for 5 min, and spun down. The denatured samples were separated by polyacrylamide gel electrophoresis, and the proteins were blotted onto nitrocellulose membranes. The membranes were first probed with the anti-FLAG and anti-Swi6 antibodies, and then with horseradish peroxidase-conjugated anti-Mouse and anti-Rabbit IgG (GE Healthcare), respectively.

II-11. Tethered transcription assay

To construct the reporter plasmid, a sequence including three Gal4-binding sites of

the *GAL10* promoter was amplified with the primers 5'-CTTGCATGCGTGAAGA CGAGGACGCAC-3' and 5'-CTCATTGCTATATTGAAGTACGG-3' from the *S. cerevisiae* W303 genome; the 154-bp region of the *nmt1* promoter, which contained core promoter sequence but lacked the thiamine regulatory element [94], was amplified with the primers 5'-CCGTACTTCAATATAGCAATGAGGCAGCGAAAC TAAAAACCG-3' and 5'-GTCGACATGATTTAACAAAGCGAC-3'; the coding sequence of *ade6-m210* was amplified with the primers 5'-CTTTGTTAAATCATGT CGACGAGCGAAAAACAGGTTGTAG-3' and 5'-TTTACCCGGGCTATGCAGAAT AATTTTTCCAACC-3' from the *S. pombe* FY648 genome. These DNA fragments were fused by the polymerase chain reaction (PCR)-based method as previously described [88]. The fused fragment was cut with *Sph*I and *Xma*I and ligated into the pSLF173 plasmid [95] digested with the same enzymes for removal of the *nmt1* promoter, and the resultant plasmid was named pGNP154-Am. To construct expression plasmids, the 3FLAG-Gal4DBD fragment was made by PCR fusion and ligated into the pREP41 plasmid with *Nde*I and *Bam*HI. The resulting plasmid was used as an empty (control) plasmid, named pNFD41. An SV40 nuclear localization signal (NLS) sequence and a multi-cloning site (MCS) were added to the 5' end of the forward and reverse primers, respectively, to amplify the Gal4DBD sequence (5'-GACAAGGGTGGTGGCTCCCCAAAAAAGAAGAGAAAGGTCGAAGACGCA ATGAAGCTACTGTCTTCTATCG-3' and 5'-TTCTGGATCCGTCGACGCGGCCG CCATGGAACCTCCTCCCGATACAGTCAACTGTCTTTG-3'). The extended Gal4DBD fragment was then fused to the 3FLAG fragment by another PCR to make the 3FLAG-Gal4DBD fragment. Target sequences, *epe1* mutants or the transactivation domain (TAD) of VP16 derived from human herpesvirus 1, were ligated into the empty plasmid with *Nco*I and *Sal*I. Not all primers used for construction of expression plasmids are shown because of the complexity. The TP4-1D strain, harboring *ade6-M216*, was transformed with reporter and expression plasmids, which contain *ura4* and *LEU2* markers, respectively. The transformants were cultured on PMG medium lacking uracil and leucine with 15 μM of thiamine. Serial dilution assay was performed using PMG medium lacking uracil, leucine, and adenine without thiamine. Control and assay plates were incubated at 30°C for 8 days.

III. Results

III-1. Loss of *epe1* induces ectopic heterochromatin formation

III-1-a. Epe1-lacking cells form atypical white colonies within variegation

To monitor the state of heterochromatin, an *ade6*$^{+}$ marker is conventionally inserted in a centromeric heterochromatin region. The strain used harbored an *otr1R::ade6*$^{+}$ marker without endogenous *ade6*, where the *ade6* gene inserted in *dg*, one of the centromeric repeats for generating siRNA, was silenced by heterochroamtin, leading to accumulation of AIR and formation of red pigment on adenine-limited medium (Figure 5A and 5B) [39, 41]. Loss of Clr4 is believed to completely disrupt heterochromatin and induce a white phenotype, but I found that the *clr4*Δ strain showed a light pink phenotype but not white in our laboratory conditions (Figure 5C and 5D). Loss of *epe1* generated a mixture of not only red and pink colonies but also white ones distinct from the *clr4*Δ-induced light pink colonies. Replating single white colonies frequently produced white colonies with some red/pink ones. I established white clones by two rounds of white-colony isolation. One of the white-isolated strains, *epe1*Δ W70, produced white colonies with a frequency of 89%. This partially reversible propagation with plasticity and persistence suggested that the white phenotype of the *epe1*Δ strain arose through an epigenetic mechanism rather than a genetic mutation.

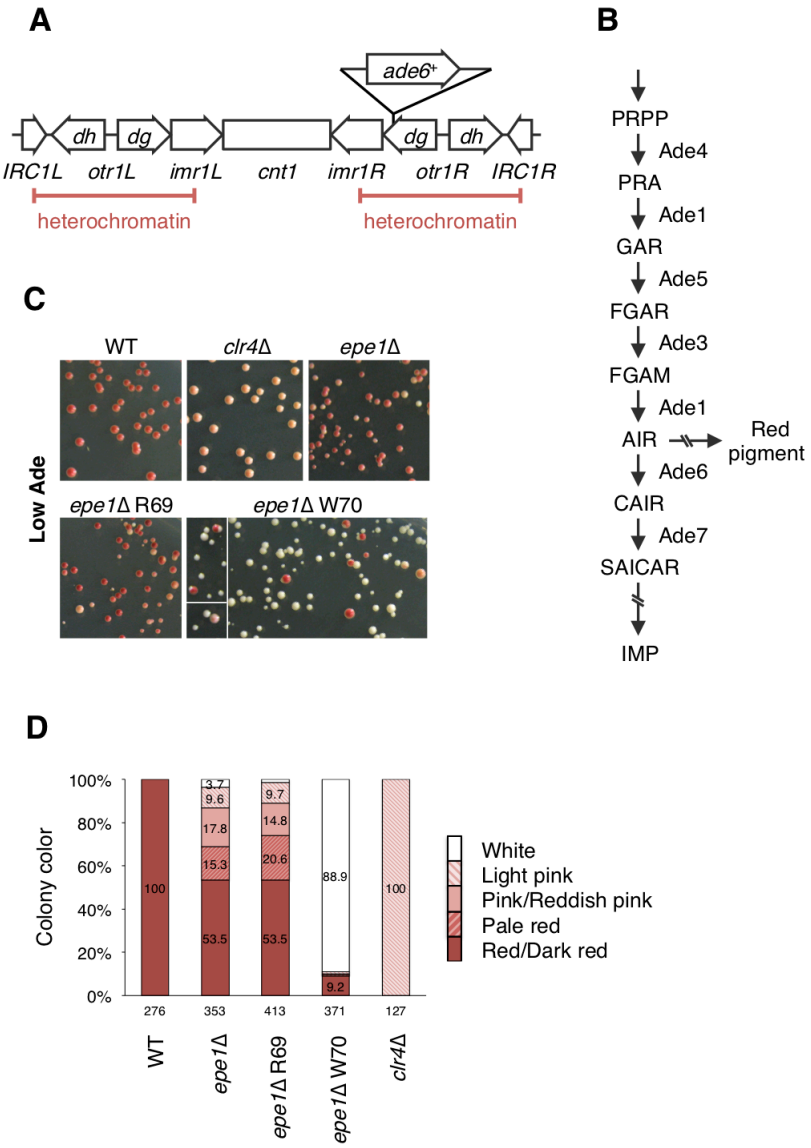

Figure 5. Epe1-lacking cells form atypical white colonies within variegation

(A) Schematic diagram showing the structure of the centromere of chromosome I (*cen1*). The position of the *ade6*$^{+}$ marker is indicated (*otr1R::ade6*$^{+}$). Endogenous *ade6* is disrupted by a loss-of-function truncation mutation (*ade6-DN/N*). (B) Biosynthetic pathway for inositol monophosphate (IMP). Ade1 is a bifunctional enzyme. Little is known about the pathway of red pigment synthesis. (C) Colony color of *epe1*Δ clones and wild-type (WT) and *clr4*Δ strains on adenine-limited (Low Ade) medium. (D) Percentage of the colored and white colonies. Total counts are shown below the graph. Colonies that were too small were excluded from the color assessment.

III-1-b. Mislocalized heterochromatin silences euchromatic genes

To investigate the mechanism for producing the white colonies, I performed ChIP analysis of H3K9me. Unlike *clr4*Δ, the *epe1*Δ W70 strain retained a substantial amount of H3K9me on *otr1R::ade6*$^{+}$ (Figure 6A). The *epe1*Δ W70 strain showed low level of expression of *otr1R::ade6*$^{+}$, which was comparable to that of the parental *epe1*Δ strain and a red-isolated strain, *epe1*Δ R69 (Figure 6B). These results suggested that the white phenotype of W70 was not linked to *otr1R::ade6*$^{+}$. To explore the cause of the white phenotype of W70, I performed microarray transcriptome analysis in W70 and R69 cells, which uncovered a cluster of genes silenced only in W70 (Figure 6C). This cluster encompassed a 23 kb euchromatic region neighboring the right subtelomere of chromosome III (*subtel3R*); this region contained the *ade5* gene, whose product acts upstream of Ade6 in IMP biosynthesis (Figure 5B). Since loss of Epe1 increases H3K9me levels at *subtel1L* and *2L* [68, 69], I hypothesized that the *ade5* gene was silenced by ectopically deposited H3K9me, which arrested red pigment formation. ChIP analysis in W70 cells revealed the presence of strong ectopic heterochromatin on *ade5* with H3K9me levels comparable to those on centromeric *ade6* in WT cells, but such ectopic heterochromatin was not detected in parental *epe1*Δ and *epe1*Δ R69 (Figure 6A). Consistently, qRT-PCR analysis revealed that W70 cells had lower *ade5* expression than WT, parental *epe1*Δ, and R69 cells (Figure 6B). In W70 cells, *ade5*-like accumulation of H3K9me was observed at neighboring *puf6* and *SPCC569.03* but not at *nsa2*, which lay outside the cluster identified by transcriptome analysis (Figure 6D). Accordingly, I detected accumulation of Swi6 at *ade5* but not at *nsa2* in W70 cells (Figure 6E). These results suggested that silencing of the *ade5* gene by strong ectopic heterochromatin formation caused the white phenotype of W70.

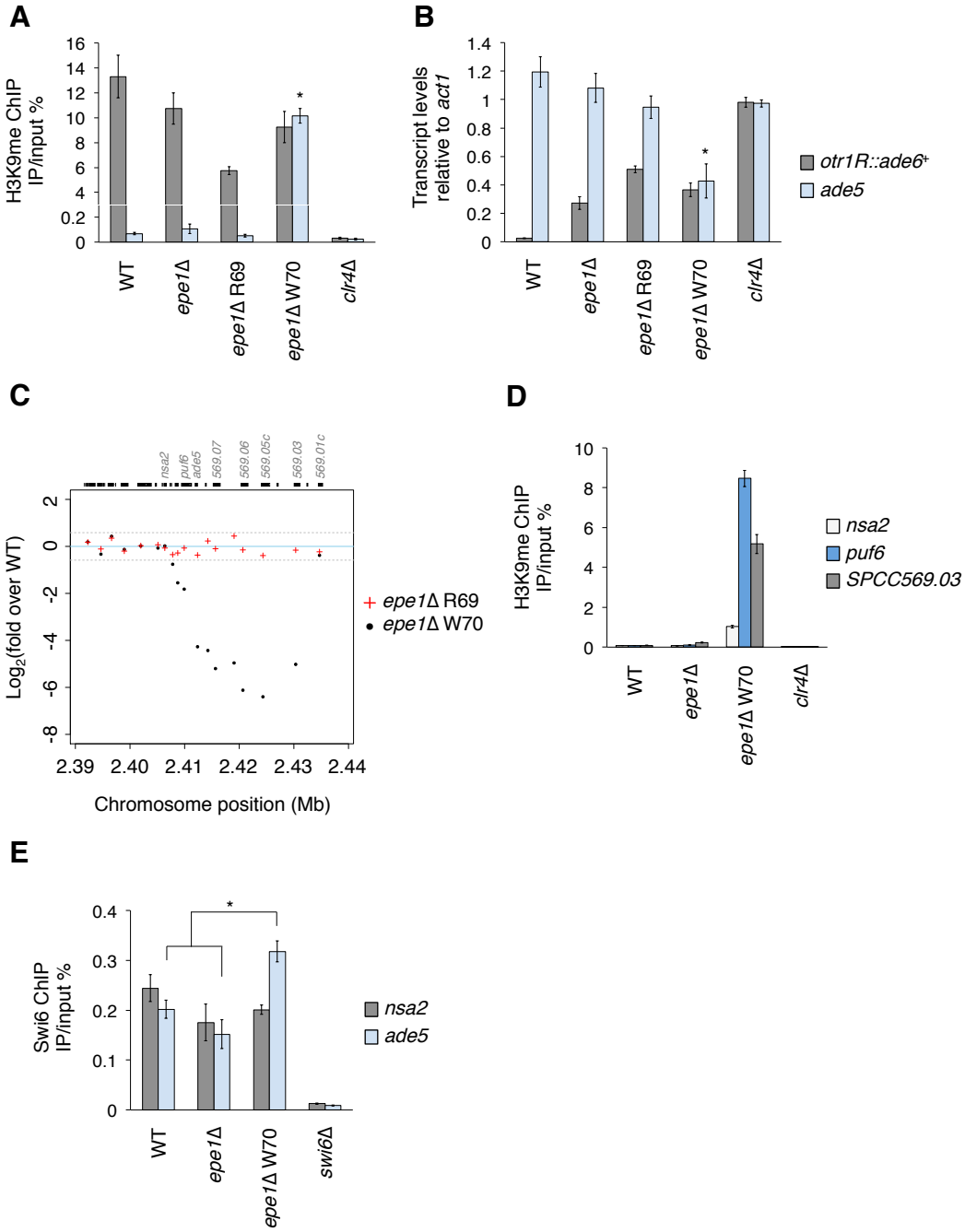

Figure 6. Mislocalized heterochromatin silences euchromatic genes

(A) Chromatin immunoprecipitation (ChIP)-qPCR analysis of H3K9me levels at *otr1R::ade6*$^{+}$ and *ade5*. *p < 0.05. p-values were determined using a two-tailed Student's t-test comparing the indicated sample value with the value of other samples. (B) Reverse transcription and quantitative polymerase chain reaction (qRT-PCR) analysis of *otr1R::ade6*$^{+}$ and *ade5* transcript levels relative to those of *act1*. *p < 0.05. p-values were determined using a two-tailed Student's t-test comparing the indicated sample value with the value of other samples. (C) Transcriptome microarray analysis. The

x-axis indicates the chromosome position of *subtel3R*. The y-axis indicates $\log_2$ fold changes of gene expression levels in R69 or W70 clone cells over those in WT cells. The upper panel indicates the gene positions and names corresponding to array positions. Unreliable signals with low intensity were excluded. Red cross, *epe1*Δ R69/WT; black dot, *epe1*Δ W70/WT; sky-blue solid line, y = 0; gray broken line, y = $\pm\log_2(1.5)$. (D) ChIP-qPCR analysis of H3K9me at *nsa2*, *puf6*, and *SPCC569.03*. (E) ChIP-qPCR analyses of Swi6 at *subtel3R* genes, *nsa2* and *ade5*. *$p < 0.05$ (two-tailed Student's *t*-test). ChIP-qPCR and qRT-PCR data in (A), (B), (D), and (E) are represented as mean ± standard deviation (SD) of three independent experiments (n = 3).

III-1-c. Ectopic heterochromatin formation at *ade5* causes a white phenotype

To confirm the cause of the white phenotype, I performed genetic complementation of the W70 strain. I developed the diploid complementation system, a gene complementation system to supply single copies of $epe1^+$ and/or $ade5^+$ by diploid cell formation (Figure 7A). Control diploid strains displayed expected phenotypes: $epe1^{+/+}$ and $epe1^{\Delta/+}$, red; $epe1^{\Delta/\Delta}$, red-white variegation; and $ade5^{\Delta/\Delta}$, completely white (Figure 7B). I designated the ectopic heterochromatin-containing allele in W70 as $ade5^*$. When the W70 strain (*epe1*Δ $ade5^*$) was mated with an *epe1*Δ *ade5*Δ strain to generate $epe1^{\Delta/\Delta}$ $ade5^{*/\Delta}$, the white phenotype of *epe1*Δ $ade5^*$ was retained, indicating that no alleles except *epe1*Δ and $ade5^*$ of W70 caused the white phenotype (Figure 7A). By contrast, introduction of $ade5^+$ complemented the white phenotype ($epe1^{\Delta/\Delta}$ $ade5^{*/+}$), showing that $ade5^*$ was responsible for the white phenotype. Similarly, provision of $epe1^+$ complemented the white phenotype of *epe1*Δ $ade5^*$ ($epe1^{\Delta/+}$ $ade5^{*/\Delta}$). ChIP analysis of these diploid cells showed the loss of H3K9me at the *ade5* region, indicating that re-introduction of Epe1 promoted demethylation of H3K9me at $ade5^*$ (Figure 7C). Thus, I concluded that ectopic heterochromatin-mediated repression of *ade5* caused the white phenotype of the *epe1*Δ W70 strain. In addition, these results showed that Epe1 removed H3K9me from spontaneously formed ectopic heterochromatin.

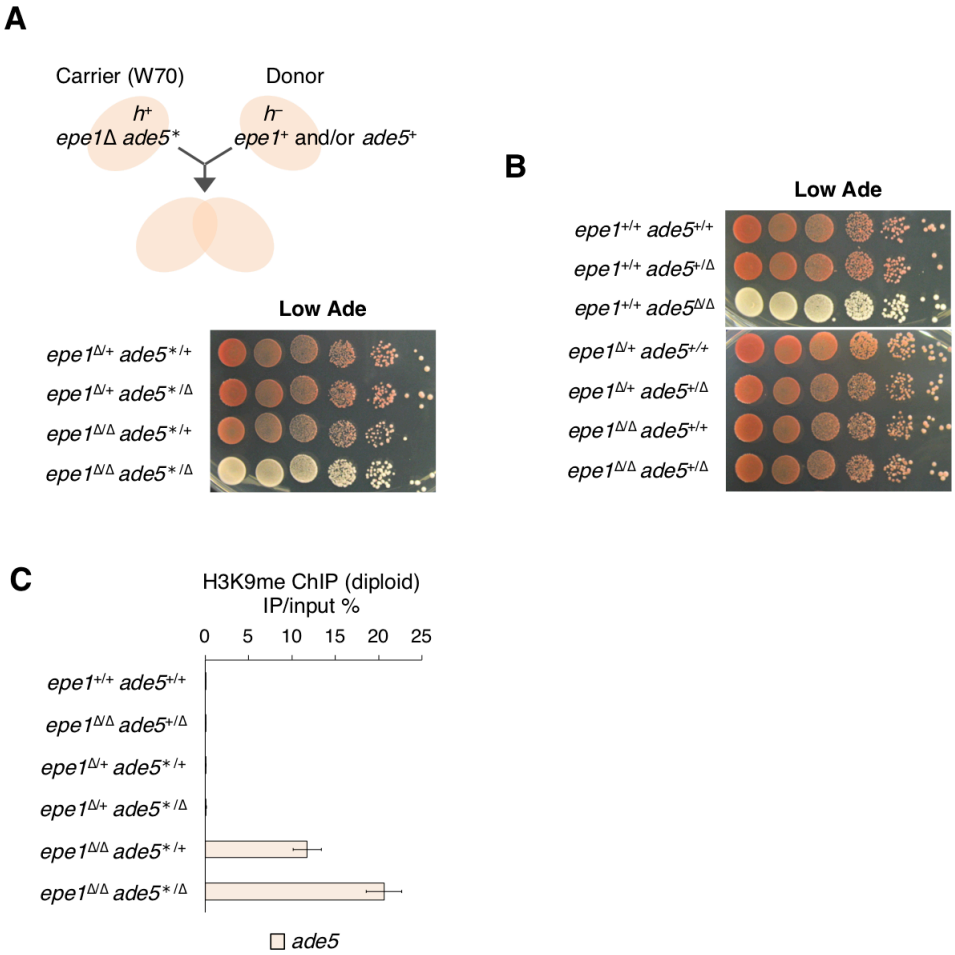

Figure 7. Ectopic heterochromatin formation at *ade5* causes a white phenotype

(A) Ten-fold serial dilution assay for diploid strains. Schematic representation of the diploid complementation system is indicated. The *epe1*Δ W70 strain was used as a carrier strain. (B) Ten-fold serial dilution assay for diploid strains. Control strains were spotted on adenine-limited medium. (C) ChIP-qPCR analysis of H3K9me at *ade5* in diploids. $ade5^{+/+}$ and $ade5^{*/+}$ samples provided biallelic signals. $ade5^{+/\Delta}$ and $ade5^{*/\Delta}$ samples provided monoallelic signals. Data are represented as mean ± standard deviation (SD) of three independent experiments (n = 3).

III-2. The red-white variegation phenotype is linked to stochastic ectopic heterochromatin formation

III-2-a. Loss of *epe1* induces a variegation phenotype unrelated to the marker gene

The strain used in Figure 5–7 has the *otr1R::ade6*$^{+}$ marker, which contributes to *epe1*Δ-induced variegation [44]. To highlight marker-independent variegation, I employed a strain harboring *ade6-m210*, a loss-of-function allele of the *ade6* gene, and

no *ade6* transgene. This strain showed a uniform red phenotype on adenine-limited medium (Figure 8A). Introduction of *epe1*Δ induced a red-white variegated phenotype with a lower proportion of pink and white colonies than that of the *epe1*Δ *otr1R::ade6*$^{+}$ strain (Fig 8A and 8B).

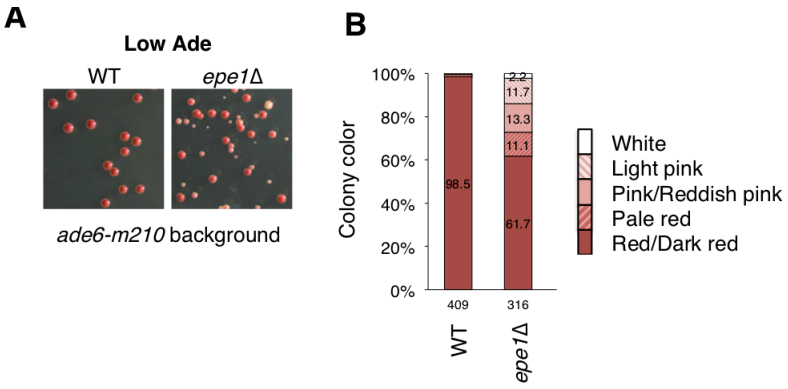

Figure 8. Loss of *epe1* induces a variegation phenotype unrelated to the marker gene

(A) Comparison of colony color on adenine-limited medium. These strains had no *ade6*$^{+}$ marker. Endogenous *ade6* is disrupted by a loss-of-function mutation (*ade6-m210*) [40]. Eight percent of the plate area is displayed. (B) Percentage of colored and white colonies of single and double deletion mutants shown in (A).

III-2-b. Ectopic heterochromatin is stochastically formed at *ade5*

To test the relationship between the red-white variegation and ectopic heterochromatin formation in the *ade6-m210* strain, I established several red- and white-isolated clones from the *ade6-m210* strain lacking *epe1*. Some white-isolated clones, W1-1, 2-1, W5-1, and W9-1, showed a white or pink phenotype, but W6-1 and W8-1 showed an *epe1*Δ-like phenotype despite white isolation, suggesting that the white phenotype is not necessarily stable thorough cell divisions (Figure 9A). The three red isolates showed an *epe1*Δ-like phenotype. Using ChIP-sequencing, I analyzed the whole genome distribution of H3K9me of several strains. The results revealed formation of strong ectopic heterochromatin on *ade5* in *epe1*Δ W1-1, W2-1, and W9-1, which was confirmed by ChIP-qPCR analysis (Figure 9B and 9C). Accordingly, *ade5* expression was decreased in the *epe1*Δ W1-1 clone (Figure 9D). These results suggest that *ade5* ectopic heterochromatin caused the appearance of white colonies of *epe1*Δ *ade6-m210* cells.

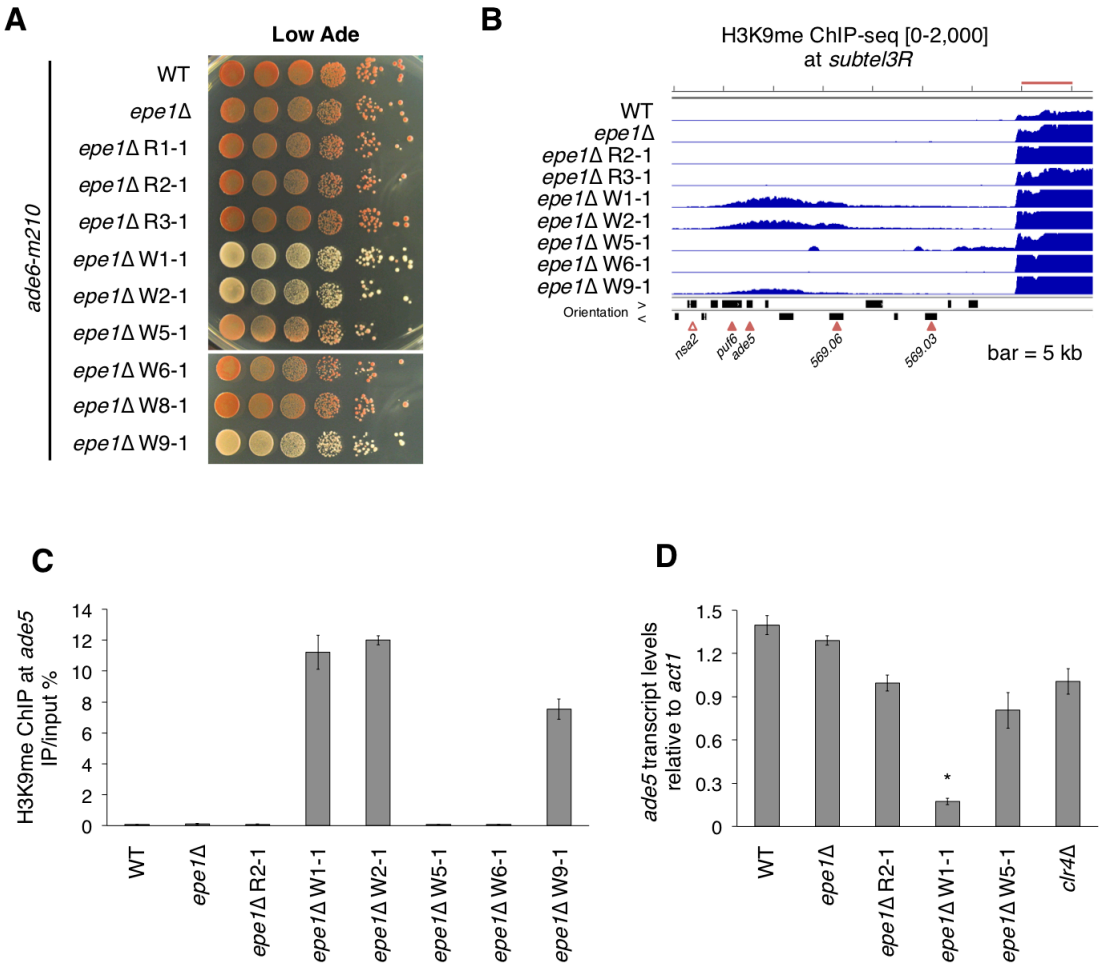

Figure 9. Ectopic heterochromatin is stochastically formed at *ade5*

(A) Ten-fold serial dilution assay. Some of the obtained isolates were spotted on adenine-limited medium. *epe1*Δ W6-1 and W8-1 clones displayed parental *epe1*Δ-like phenotypes despite white colony isolation. (B) ChIP-sequencing (ChIP-seq) analysis of H3K9me. Right subtelomeres of chromosome III are shown. Blue graphs indicate normalized fragment counts. The vertical range of the graphs is indicated on the left. Open arrowhead, essential genes based on the *S. pombe* gene database (PomBase; https://www.pombase.org); filled arrowhead, nonessential genes; orientation >, left to right; orientation <, right to left. Bar, 5 kb. (C) ChIP-qPCR analysis of H3K9me at *ade5*. (D) qRT-PCR analysis of *ade5* transcript levels. *$p < 0.05$. *p*-values were determined using a two-tailed Student's *t*-test comparing the indicated sample value with the value of other samples. ChIP-qPCR and qRT-PCR data in (C) and (D) are represented as mean ± standard deviation (SD) of three independent experiments (n = 3).

III-2-c. Ectopic heterochromatin stochastically appears at genes involved in red pigment formation

The *epe1*Δ W5-1 strain displayed a pink phenotype without increased H3K9me on *ade5*, but displayed ectopic heterochromatin formation on *ade1* and its neighboring region, and a decreased level of *ade1* expression (Figure 10A–C). Note that since *ade1* and *ade5* are located in different chromosomes, their heterochromatin formation may not be linked. Since, like Ade5, Ade1 functions upstream of Ade6 in *de novo* IMP biosynthesis (Figure 5B), the pink phenotype was probably due to ectopic silencing of *ade1*. These results suggest that white or pink colonies are generated by stochastic formation of ectopic heterochromatin at pigmentation-associated genes.

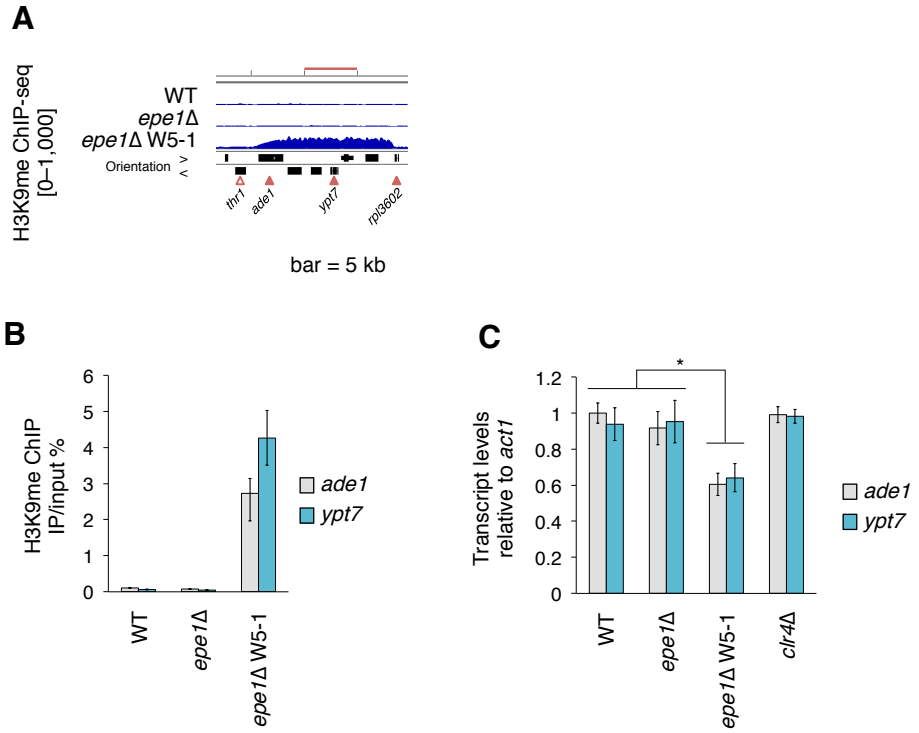

Figure 10. Ectopic heterochromatin stochastically appears at genes involved in red pigment formation

(A) ChIP-sequencing analysis of H3K9me. *ade1* and the surrounding region are shown. Bar, 5 kb; open arrowhead, essential genes based on PomBase; filled arrowhead, nonessential genes. (B) ChIP-qPCR analysis of H3K9me at *ade1* and *ypt7*. (C) qRT-PCR analysis of *ade1* and *ypt7*

transcript levels. ChIP-qPCR and qRT-PCR data in (B) and (C) are represented as mean ± SD of three independent experiments (n = 3). *$p < 0.05$ (two-tailed Student's *t*-test).

III-2-d. Variegation occurs dependently on heterochromatin assembly

However, it is unknown whether the pink and white colonies of the *epe1*Δ *ade6-m210* strain appear in a heterochromatin formation-dependent manner. To clarify this, I introduced mutations of genes required for heterochromatin formation and analyzed their effects on the *epe1*Δ-induced variegation phenotype (Figure 11A and 11B). Loss of Clr4 abolished red-white variegation in the *epe1*Δ *ade6-m210* background, indicating a requirement for the H3K9 methyltransferase Clr4. Similarly, loss of another major heterochromatin factor, Swi6, suppressed variegation (Figure 11A and 11B). These results suggest that red-white variegation relies on heterochromatin assembly.

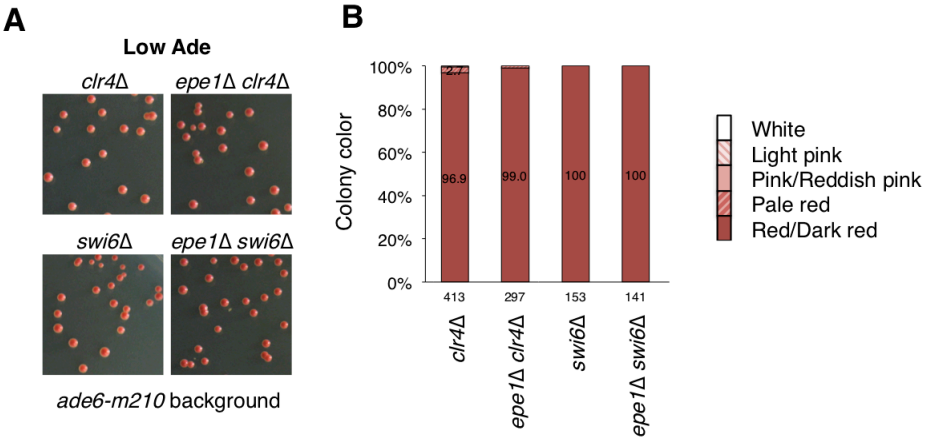

Figure 11. Variegation occurs dependently on heterochromatin assembly

(A) Comparison of colony color among double deletion mutants on adenine-limited medium. Strains with single deletions of major heterochromatin assembly factors are shown side by side. (B) Percentage of colored and white colonies of single and double deletion mutants shown in (A).

III-2-e. Ectopic heterochromatin at *subtel3R* is formed independently of the RNAi or Taz1 pathway

I found ectopic heterochromatin at *ade5* with a higher frequency than *ade1*. I hypothesized that subtelomeric constitutive heterochromatin enhanced the formation of *ade5* ectopic heterochromatin. To test this hypothesis, I constructed the *epe1*Δ *ago1*Δ *taz1*Δ strain, because Ago1 and Taz1 are involved in subtelomeric constitutive

heterochromatin formation [29]. However, the *epe1*Δ *ago1*Δ *taz1*Δ strain as well as *epe1*Δ *ago1*Δ and the *epe1*Δ *taz1*Δ strains displayed a variegation phenotype, suggesting that neither RNAi nor Taz1 was essential for *epe1*Δ-induced variegation (Figure 12A and 12B). In addition, I established red- and white-isolated clones of *epe1*Δ *ago1*Δ and the *epe1*Δ *taz1*Δ strains (Figure 12C). Note that the *ago1*Δ strain prepared as an experimental control displayed colony-size variegation, where the color of small colonies looked pale, but this mechanism is unclear. ChIP-seq analysis revealed that two clones of the white isolates, *epe1*Δ *ago1*Δ W2-1 and *epe1*Δ *taz1*Δ W7-2 strains, had ectopic heterochromatin on *ade5*, suggesting that neither RNAi nor Taz1 was essential for formation of *ade5* ectopic heterochromatin (Figure 12D).

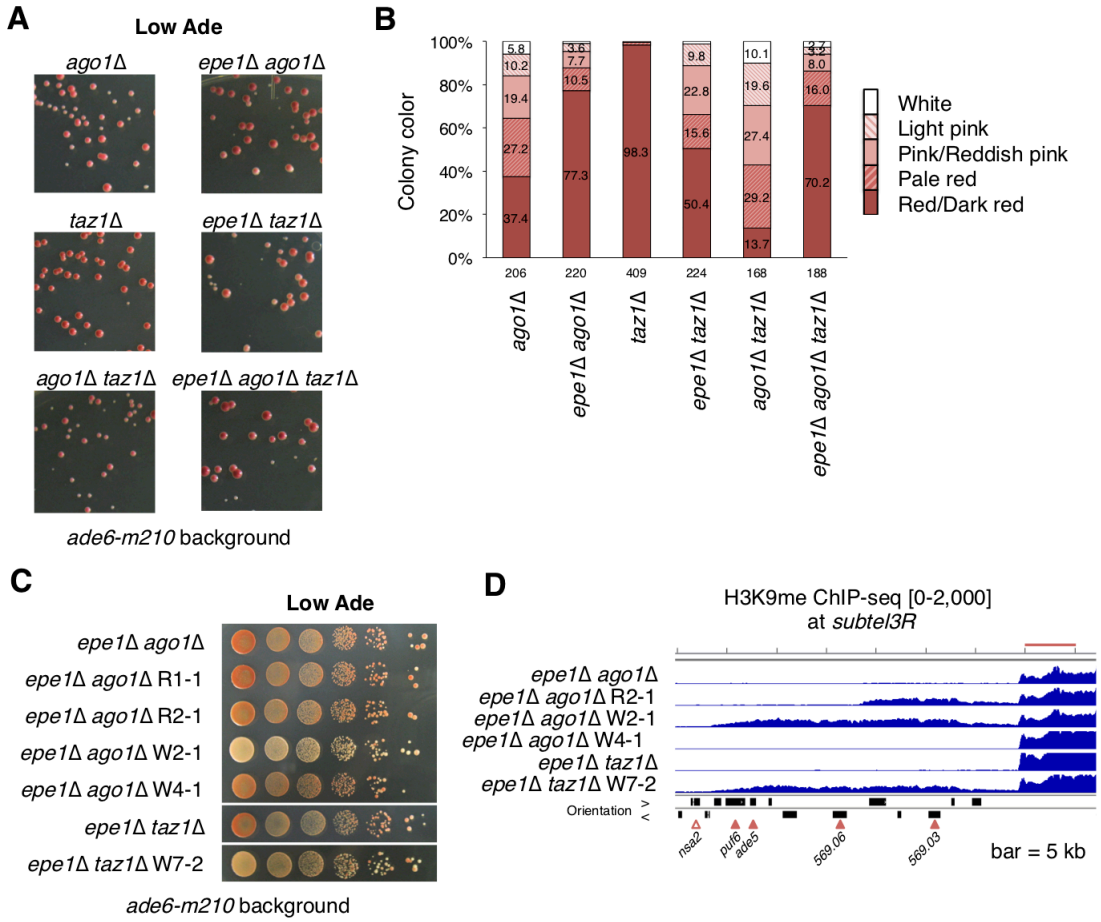

Figure 12. Ectopic heterochromatin at *subtel3R* is formed independently of the RNAi or Taz1 pathway

(A) Comparison of colony color of the strains with deletion of *ago1* and/or *taz1* with and without *epe1*Δ on adenine-limited medium. (B) Percentage of the colored and white colonies of the multiple

deletion mutants shown in (A). (C) Ten-fold serial dilution assay. Some of the isolates obtained from *epe1*Δ *ago1*Δ and *epe1*Δ *taz1*Δ strains were spotted on adenine-limited medium. (D) ChIP-sequencing (ChIP-seq) analysis of H3K9me. Right subtelomeres of chromosome III are shown. Blue graphs indicate normalized fragment counts. The vertical range of the graphs is indicated on the left. Open arrowhead, essential genes based on the *S. pombe* gene database (PomBase; https://www.pombase.org); filled arrowhead, nonessential genes; orientation >, left to right; orientation <, right to left. Bar, 5 kb.

III-3. Ectopic heterochromatin formation induces an alteration in carbon source utilization

I also performed H3K9me ChIP-seq analysis in the previously isolated W70 strain (*otr1R::ade6*$^{+}$ background). The *epe1*Δ W70 strain harbored ectopic heterochromatin not only at *subtel3R* but also at *subtel1R* (Figure 13A). I obtained another white isolate, *epe1*Δ W164, and performed ChIP-seq analysis of H3K9me (Figure 13B). Despite sharing the parental strain with W70, this strain had ectopic heterochromatin at *subtel2R* but not at *subtel1R* or *3R* (Figure 13A). This result suggested that these ectopic heterochromatin domains had been differentially established in the *epe1*Δ cell mixture. I additionally obtained a W70-like white-isolated clone from the *otr1R::ade6*$^{+}$ *epe1*Δ *ago1*Δ strain, designated as W173 (Figure 13B). In contrast to *epe1*Δ W70 and W164, *epe1*Δ *ago1*Δ W173 had ectopic heterochromatin at *subtel1R, 2R*, and *3R* (Figure 13A). Interestingly, ChIP-qPCR identified that the parental strain of *epe1*Δ *ago1*Δ W173 had ectopic heterochromatin at a *subtel2R* gene, *gal1*, but not at *ade5* (Figure 13C–E), suggesting that *subtel2R* ectopic heterochromatin already existed in the parental strain and that ectopic heterochromatin at *subtel2R* and *3R* had been established at different times. The *gal1* gene is required to utilize galactose as a carbon source. The strains harboring *gal1* ectopic heterochromatin displayed defective growth on galactose-containing medium (Figure 13F). Consistent with this analysis, *gal1* transcript levels were substantially lower in these strains than in the WT (Figure 13E). These results indicated that *gal1* ectopic heterochromatin had a gene silencing ability causing a phenotypic alteration.

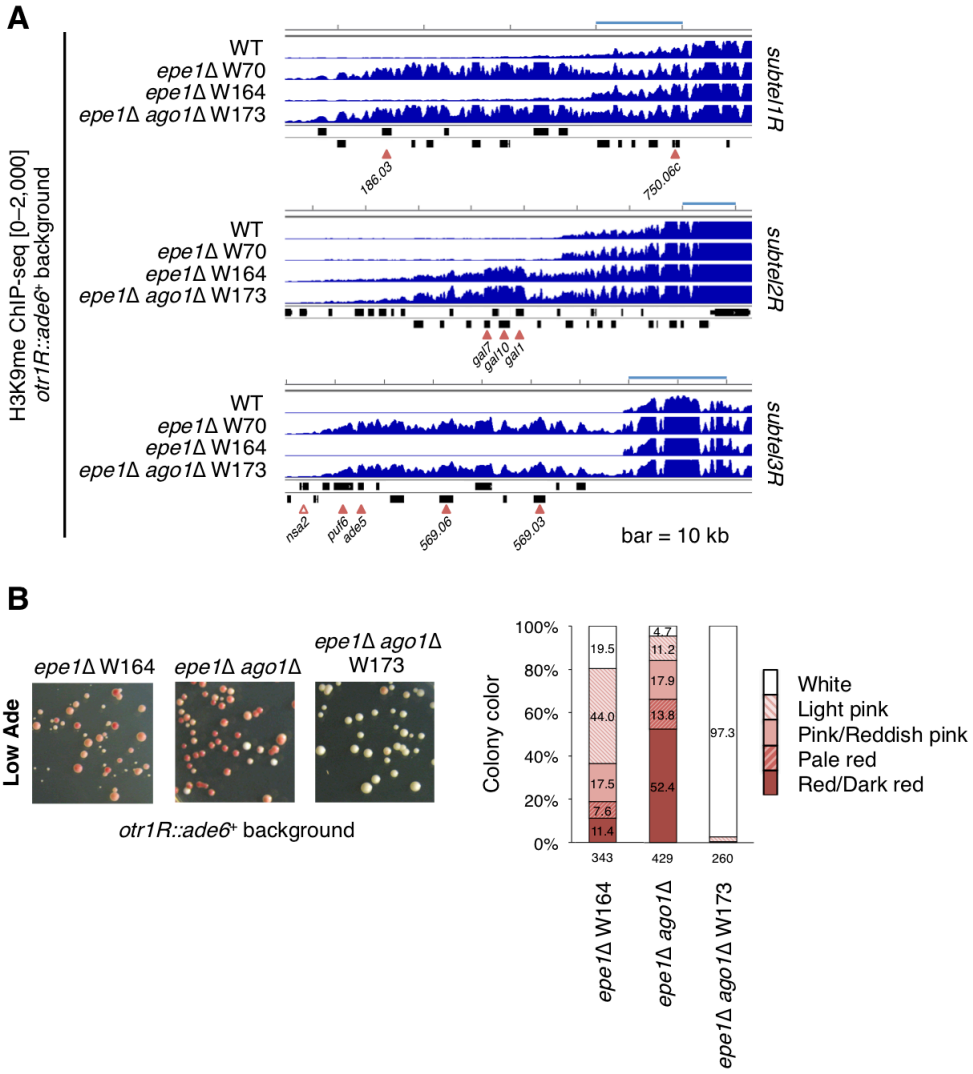
A
H3K9me ChIP-seq [0–2,000]
otr1R::ade6+ background
WT
epe1Δ W70
epe1Δ W164
epe1Δ ago1Δ W173
subtel1R
186.03
750.06c
subtel2R
gar7
gar10
gar1
subtel3R
nsa2
puf6
ade5
569.06
569.03
bar = 10 kb
B
epe1Δ W164
epe1Δ ago1Δ
epe1Δ ago1Δ W173
Low Ade
otr1R::ade6+ background
Colony color
100%
80%
60%
40%
20%
0%
19.5
44.0
17.5
7.6
11.4
4.7
11.2
17.9
13.8
52.4
97.3
343
429
260
White
Light pink
Pink/Reddish pink
Pale red
Red/Dark red
epe1Δ W164
epe1Δ ago1Δ
epe1Δ ago1Δ W173

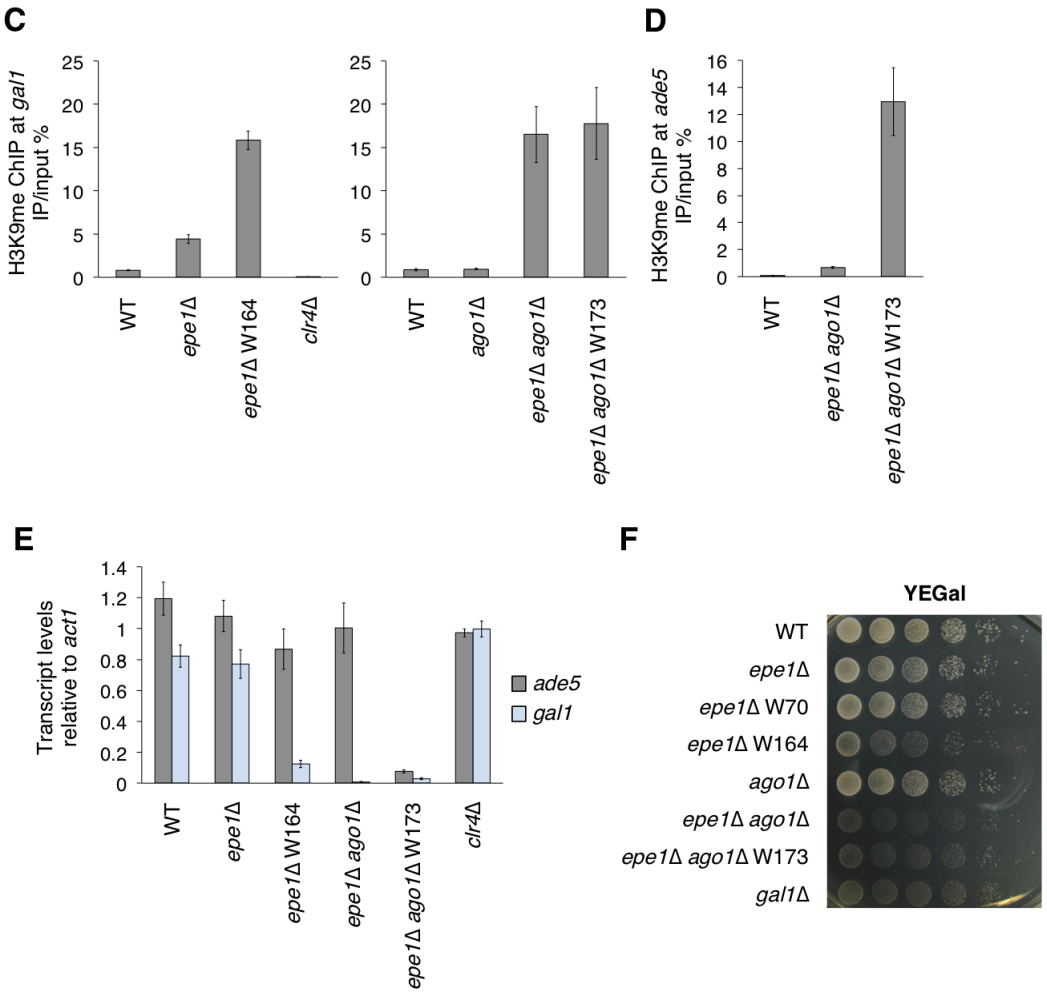

Figure 13. Ectopic heterochromatin formation induces an alteration in carbon source utilization

(A) ChIP-sequencing analysis of H3K9me in *otr1R::ade6*$^{+}$ strains. Three right subtelomeric regions are shown. The vertical range of the graphs is indicated on the left. Bar, 10 kb; open arrowhead, essential genes based on the *S. pombe* gene database; filled arrowhead, nonessential genes; orientation >, left to right; orientation <, right to left. (B) Colony color of *epe1*Δ W164, *epe1*Δ *ago1*Δ, and *epe1*Δ *ago1*Δ W173 strains on adenine-limited (Low Ade) medium (left). *epe1*Δ W164 and W70 clones share the same parental strain. Percentage of the colored and white colonies of strains is shown to the right. (C) ChIP-qPCR analyses of H3K9me at *gal1* in *epe1*Δ W164 and *epe1*Δ *ago1*Δ W173 clones. (D) ChIP-qPCR analysis of H3K9me at *ade5* in the *otr1R::ade6*$^{+}$ *epe1*Δ *ago1*Δ W173 clone. (E) qRT-PCR analysis of *ade5* and *gal1* transcript levels. (F) Ten-fold serial dilution assay on YEGal medium. ChIP-qPCR and qRT-PCR data in (C), (D), and (E) are represented as mean ± standard deviation (SD) of three independent experiments (n = 3).

III-4. Development of heterochromatin islands and formation of ectopic heterochromatin constitute the diversified epigenotypes of the *epe1*Δ strain

III-4-a. Heterochromatin islands develop heterogeneously

Loss of Epe1 increases H3K9me levels at heterochromatin islands [32, 45, 68–70]. ChIP-seq analysis revealed that a large amount of H3K9me stochastically accumulated among isolated *epe1*Δ and *epe1*Δ *ago1*Δ clones harboring the *ade6-m210* background (for example, *Is 3*, *8*, *19* in Figure 14), suggesting that heterochromatin islands had heterogeneously developed in the parental strains.

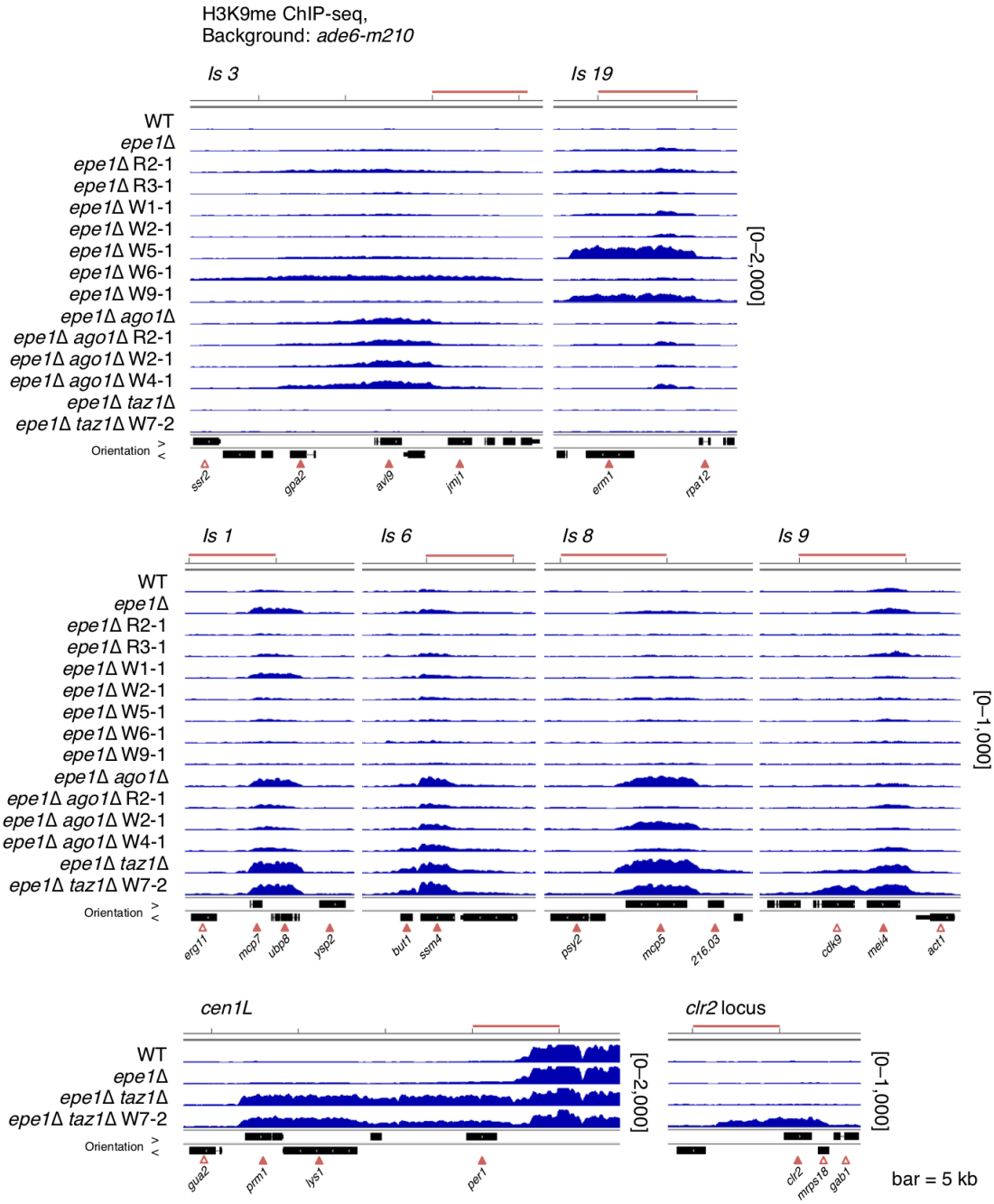

Figure 14. Heterochromatin islands develop heterogeneously

ChIP-sequencing analysis of H3K9me in *ade6-m210* clones. Heterochromatin island positions and *cen1L* and *clr2* regions are shown. Data are shown as normalized fragment counts. Bar, 5 kb; open arrowhead, essential gene based on PomBase; filled arrowhead, nonessential gene.

III-4-b. Genome-wide *de novo* heterochromatin formation takes place in every cell

The red-isolated *epe1*Δ R2-1, white-isolated *epe1*Δ *ago1*Δ W2-1, and *epe1*Δ *taz1*Δ W7-2 clones harbored ectopic heterochromatin on pigmentation-unrelated genes, *pdi4*, *can1*, and *clr2*, respectively, each of which did not correspond to known euchromatic H3K9me peaks [68, 69, 72, 75, 76, 78, 84, 85], and had no H3K9me in the parental stain (Figure 14, 15A, and 15B). This suggests that unknown potential H3K9me sources still existed in the *S. pombe* genome and strong ectopic heterochromatin can be established at these source-positive sites. Note that some of the reported islands were hardly detected in the WT strains (for example, *Is 3*, *19* in Figure 14), suggesting that some islands are inconsistently activated.

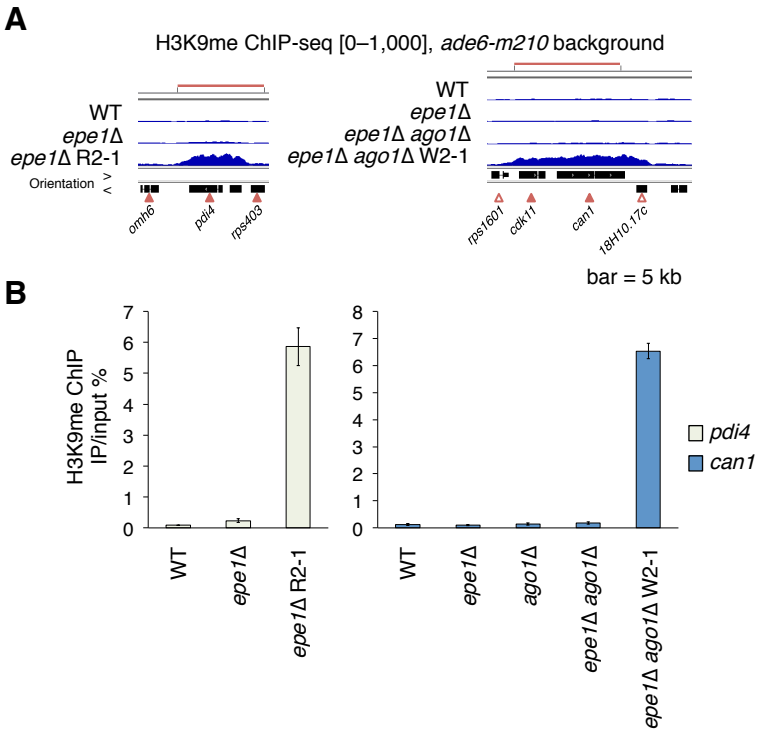

Figure 15. Genome-wide *de novo* heterochromatin formation takes place in every cell

(A) ChIP-sequencing analysis of H3K9me. *pdi4* and *can1* and their surrounding regions are shown. Bar, 5 kb. (B) ChIP-qPCR analyses of H3K9me at *pdi4* and *can1*. Data in are represented as mean ± standard deviation (SD) of three independent experiments (n = 3).

III-4-c. Epigenetic state can be changed in the presence of Epe1

It is noteworthy that the *subtel1R* heterochromatin landscape was different between the WT (*epe1*$^{+}$) strains (Figure 13A and Figure 16): despite harboring similar genetic backgrounds, the WT *ade6-m210* strain harbored extended subtelomeric heterochromatin, which was not detected in the WT *otr1R::ade6*$^{+}$ strain. The result indicates that the epigenetic profile varies between the WT strains even though they have functional Epe1. Each *epe1*-null cell had a distinct epigenotype and *epe1*$^{+}$ cells can epigenetically diverge.

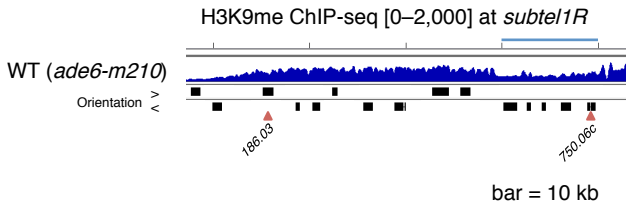

Figure 16. Epigenetic state can be changed in the presence of Epe1

ChIP-sequencing analysis of H3K9me in the *ade6-m210* WT strain. *subtel1R* is displayed. Bar, 10 kb.

III-5. Epe1 prevents ectopic heterochromatin-mediated red-white variegation via a JmjC domain-independent mechanism

III-5-a. Epe1 suppresses red-white variegation without its JmjC domain

Since Epe1 promotes demethylation of artificially deposited H3K9me *in vivo* in a JmjC domain-dependent mechanism [56, 57], I asked whether Epe1 demethylation plays a role in suppression of the red-white variegation observed in Figure 8. To examine this, I generated strains expressing N-terminal tagged wild-type Epe1 (3FLAG-Epe1) and Epe1H297A, which harbors an alanine substitution at the first Fe^{2+}-binding residue [44, 47]. H297A is a canonical catalytic-dead mutant that lacks *in vivo* demethylation activity on artificially deposited H3K9me [56, 57]. Both proteins were expressed from the endogenous *epe1* promoter and displayed almost the same protein expression levels (Figure 17A). Unlike loss of Epe1, the H297A mutation generated few pink/white colonies in the *ade6-m210* background (Figure 17B); indeed,

96.2% of Epe1H297A cells formed WT-like red colonies, while 61.7% of *epe1*Δ cells did. This result indicates that Epe1 almost fully suppressed ectopic heterochromatin-mediated variegation in a JmjC domain-independent manner.

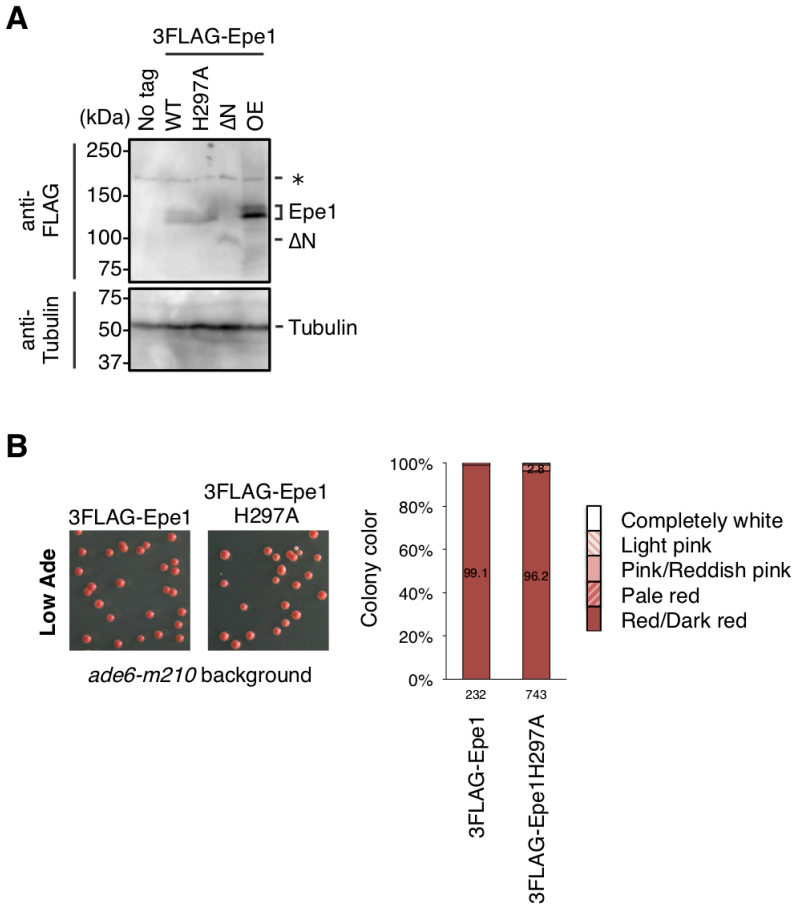

Figure 17. Epe1 suppresses red-white variegation without its JmjC domain

(A) Expression of 3FLAG-tagged Epe1 and its mutants. Proteins extracted from cells expressing the indicated types of FLAG-tagged Epe1 were separated by 6% polyacrylamide gel and analyzed by Western blotting with an antibody against FLAG (upper panel). WT cells were used as the no tag control. *, non-specific band. As a loading control, α-tubulin was used (lower panel). The samples subjected to the two antibodies were identical. (B) Comparison of colony color of strains expressing the 3FLAG-tagged Epe1 protein and H297A JmjC domain mutant on adenine-limited medium (left). Eight percent of the plate area is displayed. Percentage of colored and white colonies is shown to the right.

III-5-b. The Epe1 JmjC domain is required for removal of already-established ectopic heterochromatin

I have already shown that introduction of *epe1*$^{+}$ into W70 cells led to a red phenotype via the removal of H3K9me at *ade5** (Figure 7); however, Epe1 suppressed variegation independently of JmjC activity. Thus, I asked whether the JmjC domain is required for the removal of H3K9me at *ade5**, using a diploid complementation assay (Figure 18A). I constructed a carrier strain (*epe1*Δ W-t1) bearing *ade5* ectopic heterochromatin (*ade5**) transferred from the *epe1*Δ *ago1*Δ W173 strain, and confirmed the retention of *subtel3R* ectopic heterochromatin including *ade5** after sexual reproduction (Figure 18B and 18C). Introduction of *epe1H297A* as well as *epe1*Δ into *epe1*Δ W-t1 resulted in diploid cells that retained the white phenotype and H3K9me at *ade5**, while introduction of *epe1*$^{+}$ complemented the white phenotype and almost fully depleted H3K9me of *ade5** (Figure 18D and 18E). Furthermore, since the anti-H3K9me antibody recognizes mono-, di-, and tri-methylated H3K9, I tested whether *ade5* ectopic heterochromatin contained di- and tri-methylation marks. I detected ectopic H3K9me2 and me3 signals at *ade5* and found that their levels were substantially reduced in Epe1-introduced diploid cells (Figure 18F). These results indicate that Epe1 promoted demethylation of methyl-H3K9 including H3K9me2 and me3 at ectopic heterochromatin in a JmjC-dependent manner. However, despite of the loss of its demethylation function, Epe1H297A suppressed ectopic heterochromatin-mediated variegation (Figure 17B). These results therefore suggested that Epe1 had a JmjC domain-independent function that suppressed ectopic heterochromatin formation before accumulation of large amounts of H3K9me.

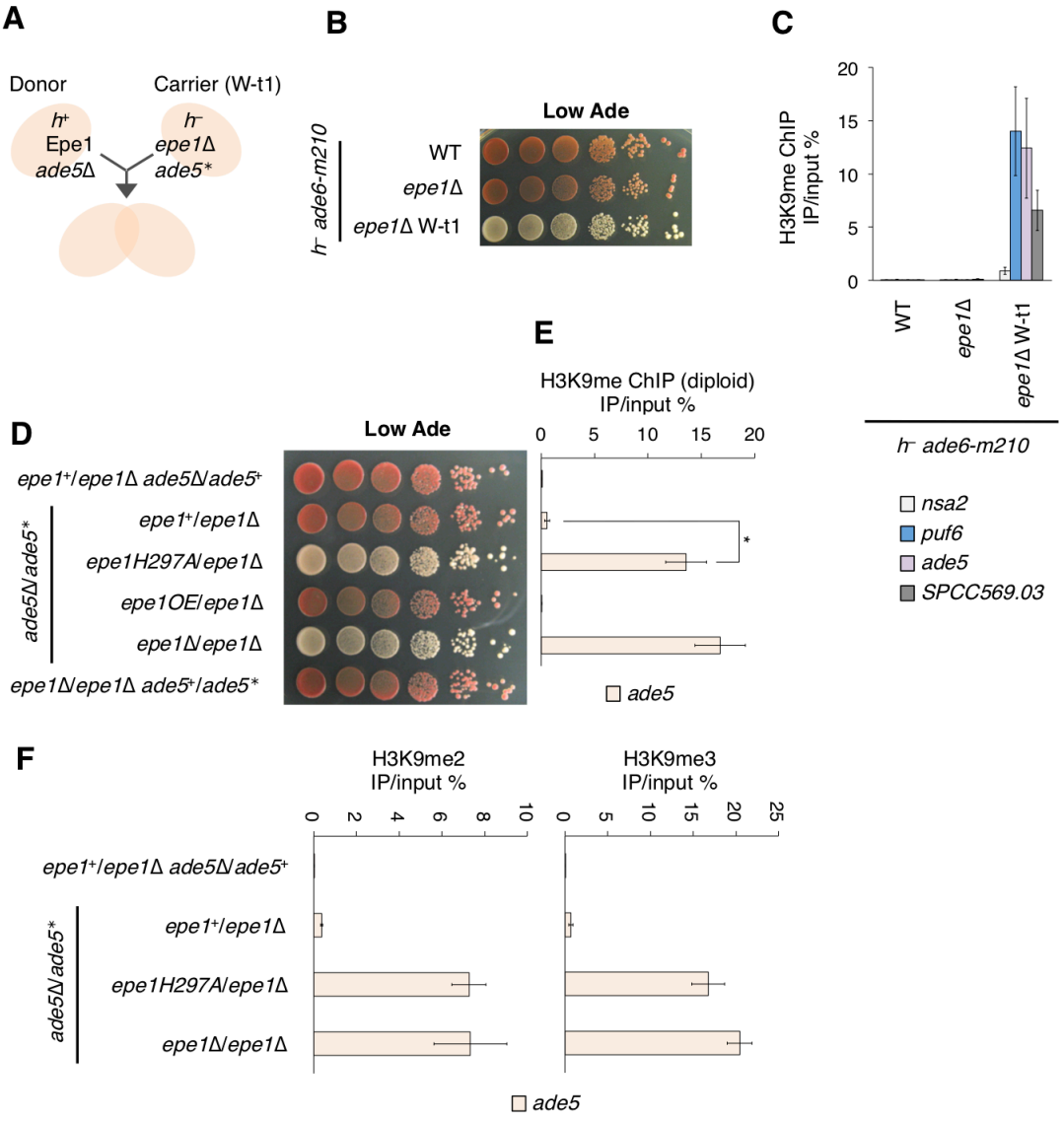

Figure 18. The Epe1 JmjC domain is required for removal of already-established ectopic heterochromatin

(A) Schematic representation of the diploid complementation analysis. The *epe1*Δ W-t1 strain was used as a carrier strain, which harbored *ade5* ectopic heterochromatin (*ade5**). (B) Ten-fold serial dilution assay of the *ade5**-transferred strain (*ade6-m210 epe1*Δ W-t1) on adenine-limited medium. (C) ChIP-qPCR analysis of H3K9me in the *ade5**-transferred strain at *nsa2*, *puf6*, *ade5*, and *SPCC569.03*. (D) Ten-fold serial dilution assay for diploid strains. The indicated strains were spotted onto adenine-limited medium. (E) ChIP-qPCR analysis of H3K9me for diploid cells at *ade5*. The qPCR signals were monoallelic. *$p < 0.05$ (two-tailed Student's *t*-test). (F) ChIP-qPCR analyses of H3K9me2 (left) and me3 (right) in diploid cells. qPCR signals at *ade5* were monoallelic.

ChIP-qPCR data in (C), (E), and (F) are represented as mean ± standard deviation (SD) of three independent experiments (n = 3).

III-6. N-terminal transcriptional activation domain is involved in the prevention of ectopic heterochromatin formation

III-6-a. The NTA domain is required for suppression of variegation

In the budding yeast-based two-hybrid system, the Epe1 protein expressed as bait activates transcription of reporter genes without prey [63] (Figure 19A). I found that deletion of the N-terminal 171 amino acids (Epe1ΔN) abolished transcriptional activation by Epe1, and the N-terminal 208 amino acids (Epe1N208) activated transcription of the *HIS3* reporter independently of JmjC (Figure 19A), suggesting that the N-terminal 171 amino acids region is required for the transcriptional activation activity in budding yeast. Since the mechanism for transcriptional activation is generally conserved among eukaryotes, I predicted that the N-terminal region of Epe1 would function as a transcriptional activation domain in fission yeast. To examine this, I established a plasmid-based reporter system (Figure 19B). I constructed a reporter plasmid containing the coding sequence of *ade6-m210* transcribed from 154 bases of the *nmt1* promoter combined with three copies of Gal4 binding sites instead of its thiamine regulatory element [94]. I also constructed expression plasmids for expressing Epe1 or its mutants fused to the Gal4 DNA binding domain (Gal4DBD). These plasmids were introduced into a fission yeast strain harboring the *ade6-M216* allele. Since *ade6-m210* and *ade6-M216* alleles show intragenic complementation, cells expressing *ade6-m210* would grow on medium without adenine, like *ade6*$^{+}$ cells. Indeed, cells expressing the VP16 transactivation domain (TAD), a well-characterized and conserved transcriptional activation domain, fused to Gal4DBD grew on medium without adenine, while cells expressing Gal4DBD alone did not (Figure 19B). Cells expressing Epe1, Epe1H297A, and NTA fused to Gal4DBD, but not Epe1ΔN, showed Ade^{+} phenotypes (Figure 19B). This indicated that the NTA domain (1–171 amino acids region) harbored transcriptional activation activity in fission yeast. Note that expression of Gal4DBD-VP16TAD or -NTA fusion protein induced growth defect on the control plate, which is likely caused by off-target effects of Gal4DBD fusion proteins with a strong activation domain. I introduced Epe1ΔN into *ade6-m210* cells to examine the

effect of the ΔN mutation on the suppression of ectopic heterochromatin formation. Epe1ΔN cells formed pink/white colonies with a slightly lower frequency than *epe1*Δ cells (Figure 19C), indicating that the NTA domain contributed to the suppression of ectopic heterochromatin-mediated variegation.

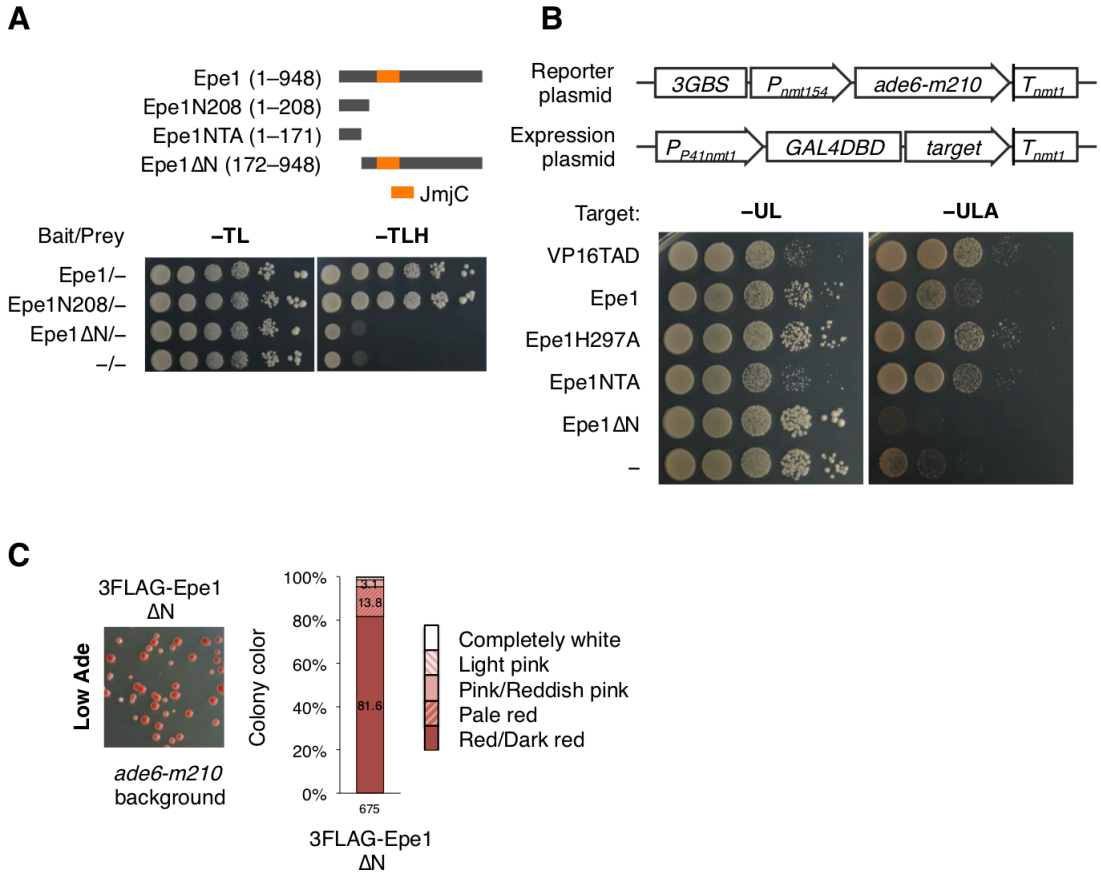

Figure 19. The NTA domain is required for suppression of variegation

(A) Analysis of transcriptional activation activity of Epe1 using the *HIS3* reporter gene in the yeast two-hybrid system. Ten-fold serial dilution assay was performed. Epe1 or its truncated mutants were expressed as bait. No protein was expressed as prey. The position of the JmjC domain is indicated in the truncation map. (B) Tethered transcription analysis of the *ade6-m210* reporter in fission yeast. Ten-fold serial dilution assay was performed. Strains containing indicated reporter and expression plasmids were spotted on PMG-based synthetic media. Minus UL, lacking Ura and Leu; −ULA, lacking Ura, Leu, and Ade. The reporter plasmid contained three Gal4-binding sites (*3GBS*) derived from the *GAL1-10* upstream activating sequence. Target peptides indicated were fused to Gal4 DNA binding domain (DBD). The VP16 transactivation domain (TAD) was used as a positive control. NTA, N-terminal transcriptional activation domain (1–171 amino acids region). (C) Colony color of

a strain expressing the 3FLAG-tagged Epe1ΔN protein (left). This strain harbored the *ade6-m210* background. Percentage of colored and white colonies is shown (right).

III-6-b. Epe1 prevents ectopic heterochromatin formation independently of its heterochromatin association activity

I performed co-immunoprecipitation analysis of Swi6 with Epe1ΔN and found that Epe1ΔN interacted with Swi6 with much lower efficiency than wild-type Epe1 (Figure 20A). However, the previous report mentions that the interaction site of Epe1 with Swi6 exists in its C-terminal one-third region [44]. Consistent with this report, the C-terminal half of Epe1 (487–948 amino acids region) interacted with Swi6 in the yeast two-hybrid system, but the N-terminal half (1–486) did not (Figure 20B). These results suggested that the interaction of Epe1 with Siw6 could be affected by an alteration in the N-terminal region apart from the interaction surface. I also asked whether Epe1H297A affected the Epe1-Swi6 interaction. The Epe1H297A mutant interacted with Swi6 with a slightly lower efficiency than wild-type Epe1 in co-IP analysis (Figure 20A). Furthermore, I examined whether the H297A mutation affected Epe1 localization at heterochromatin. FLAG ChIP analysis revealed that H297A reduced appreciably Epe1 enrichment on centromeric *dg* repeats and *IRC3* (Figure 20C), a centromeric boundary sequence where Epe1 accumulates to a high level [43, 64]. By contrast, H3K9me was maintained at *IRC3* and *dg* (Figure 20D). Although the Swi6 level was significantly reduced, it was still present at both regions (Figure 20E), suggesting that the reduced Swi6 level may not have been the primary cause of the drastic reduction in Epe1H297A enrichment on heterochromatin. These results suggested that heterochromatin association of Epe1 required anther mechanism distinct from the interaction with Swi6. Since Epe1H297A suppressed variegation, heterochromatin association activity of Epe1 was not important for the JmjC-independent prevention of ectopic heterochromatin formation.

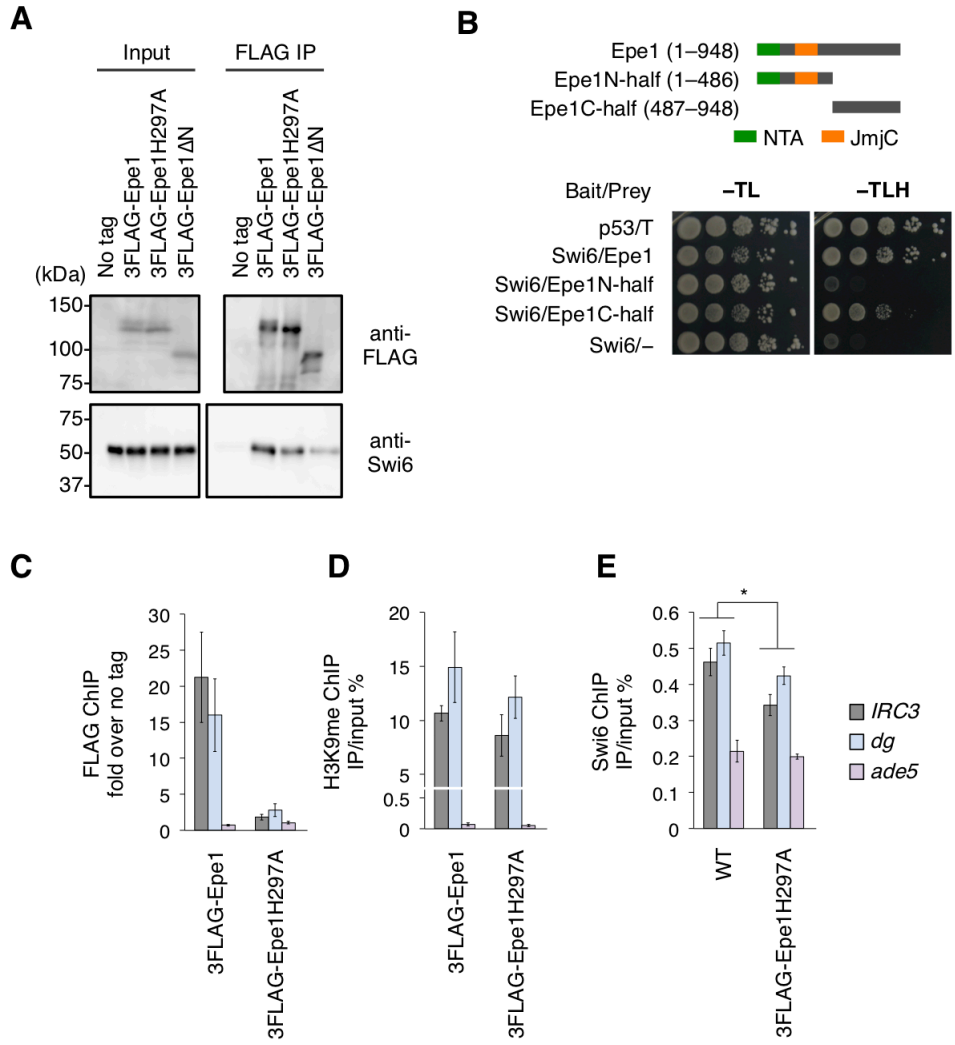

Figure 20. Epe1 prevents ectopic heterochromatin formation independently of its heterochromatin association activity

(A) Co-immunoprecipitation of Swi6 with Epe1 or its mutants. Immunoprecipitated Epe1 and Swi6 were detected by Western blotting. Input represents 20% (FLAG) or 0.4% (Swi6) of the amount of lysates used for immunoprecipitation. (B) Yeast two-hybrid analysis of the *HIS3* reporter gene. Minus TL, lacking Trp and Leu; −TLH, lacking Trp, Leu, and His. (C) ChIP-qPCR analysis of FLAG-tagged Epe1 proteins at *IRC3*, *dg*, and *ade5*. *IRC3*, the boundary sequence located outside *cen3*. WT cells were used for the no tag control. (D–E) ChIP-qPCR analyses of H3K9me (D) and Swi6 (E) at *IRC3*, *dg*, and *ade5*. *$p < 0.05$ (two-tailed Student's *t*-test). ChIP-qPCR data in (C), (D), and (E) are represented as mean ± standard deviation (SD) of three independent experiments (n = 3).

III-7. JmjC-mediated incomplete suppression of ectopic heterochromatin provides metastable epigenetic variation

III-7-a. Epe1 counteracts persistent ectopic heterochromatin in a dose-dependent manner

As shown in Figure 18E, introduction of a single copy of *epe1*$^{+}$ almost completely removed H3K9me on *ade5**. However, H3K9me on *SPCC569.03*, a *subtel3R* gene, was maintained after introduction of *epe1*$^{+}$ (Figure 21). Importantly, no H3K9me accumulation was observed on *SPCC569.03* before deletion of *epe1* (Figure 6D), indicating that ectopic heterochromatin formation at *subtel3R* was a partially irreversible epigenetic alteration. I next asked whether an increase in the level of Epe1 would reduce persistent ectopic H3K9me. Introduction of an Epe1 overexpression (Epe1OE) allele achieved complete removal of H3K9me on *SPCC569.03*, suggesting that the amount of Epe1 is critical for the removal of residual H3K9me (Figure 21).

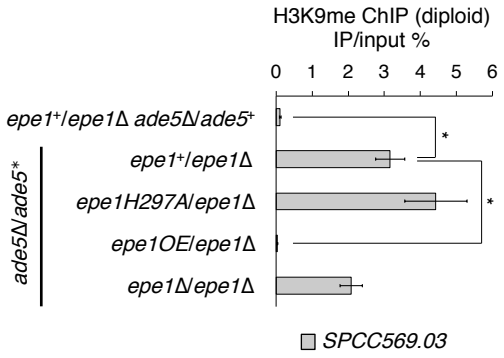

Figure 21. Epe1 counteracts persistent ectopic heterochromatin in a dose-dependent manner

ChIP-qPCR analysis of H3K9me at *SPCC569.03* in diploid cells. The indicated strains provided biallelic signals. *$p < 0.05$ (two-tailed Student's *t*-test). The strains used were the same as those in Figure 18D and 18E.

III-7-b. JmjC-mediated incomplete removal function allow retention of ectopic heterochromatin

After re-introduction of a single copy of Epe1 into *epe1*Δ *ade5** cells, I observed a difference in persistent H3K9me levels between *ade5* and *SPCC569.03*, both of which had not undergone H3K9me deposition in the presence of Epe1 (Figure 18E and Figure

21). Since *SPCC569.03* is close to subtelomeric constitutive heterochromatin, I speculated that Epe1 would not remove already-established heterochromatin neighboring a constitutive supply source of H3K9me. To investigate this, I used a mild H3K9me source that does not deposit H3K9me in the presence of Epe1 but does in the absence of Epe1. Taz1, a subunit of the telomere protection complex Shelterin, binds to telomeric repeats [30, 89]. Five heterochromatin islands harbor 2–5 copies of telomere repeat units coupled with a late replication origin, which recruit Clr4 via Shelterin to deposit H3K9me [31, 32]. Thus, I predicted that low numbers of telomere repeats lacking the late origin would induce little or no H3K9me accumulation when Epe1 was present, but initiate H3K9me deposition when Epe1 was absent. I constructed a Taz1-binding cassette (*LEU2-4TBS*), which consists of the coding sequence (CDS) of *S. cerevisiae LEU2* and four copies of a unit of telomere repeats [89, 90], and introduced it into the *ade6-m210* background strain, where it was inserted after the *SPCC569.06* promoter, a location distant from *ade5* (Figure 22A). *S. cerevisiae LEU2* functions in place of *S. pombe leu1*. The inserted *LEU2* complemented the *leu1*$^{-}$ allele harbored by the *ade6-m210* strains, resulting in growth on −Leu medium (Figure 22B). The *epe1*Δ *LEU2-4TBS* strain displayed marginal growth retardation on −Leu medium, indicating that *4TBS* did not strongly silence *LEU2* even in the absence of Epe1. This strain also showed red-white variegation. White colony isolation constantly generated clones that displayed Leu^{-} and irreversible white phenotypes. One of the clones, *epe1*Δ *LEU2-4TBS* W1-1, harbored higher H3K9me deposition on *ade5* and *LEU2* (Figure 22B and 22C). I designated the silenced *ade5* and *LEU2* alleles as *ade5** and *LEU2**, respectively. Diploid-based complementation showed that introduction of wild-type Epe1 resulted in a red colony and Leu^{-} phenotype (Figure 22D and 22E). Consistently, H3K9me on *ade5* was almost completely removed, whereas that on *LEU2* was not reduced by the provision of a single copy of Epe1 (Figure 22F), suggesting that Epe1 failed to antagonize heterochromatin neighboring the H3K9me source but greatly decreased H3K9me levels at non-contiguous locations. By contrast, introduction of Epe1OE resulted in a red colony and Leu^{+} phenotype and the complete removal of *subtel3R* ectopic H3K9me, indicating that Epe1OE overcame *4TBS*-induced self-retaining heterochromatin. Constitutive heterochromatin harboring a strong maintenance system such as RNAi, in contrast to weak systems such as *4TBS*, withstands Epe1 overexpression to some extent [43, 45,]. Our results suggest that the

balance between the level of Epe1 and intensity of the self-maintenance system in each domain determines the extent of heterochromatin retention. Importantly, *LEU2-4TBS* deposited no H3K9me on *LEU2* or *ade5* in the *epe1*$^{+}$ background, whereas accumulation was obvious in *epe1*Δ (Figure 22C). This strongly suggests the existence of a mechanism for the retention of altered chromatin structure, in which Epe1 suppresses *de novo* ectopic heterochromatin establishment, but after establishment via escape from suppression, the ectopic heterochromatin is retained by the latent H3K9me source despite the presence of Epe1. In summary, I reveal that Epe1 allows retention of robust ectopic heterochromatin, in which the level of persistent ectopic H3K9me is determined by the amount of Epe1, the distance between target H3K9me and the H3K9me source, and the intensity of the source.

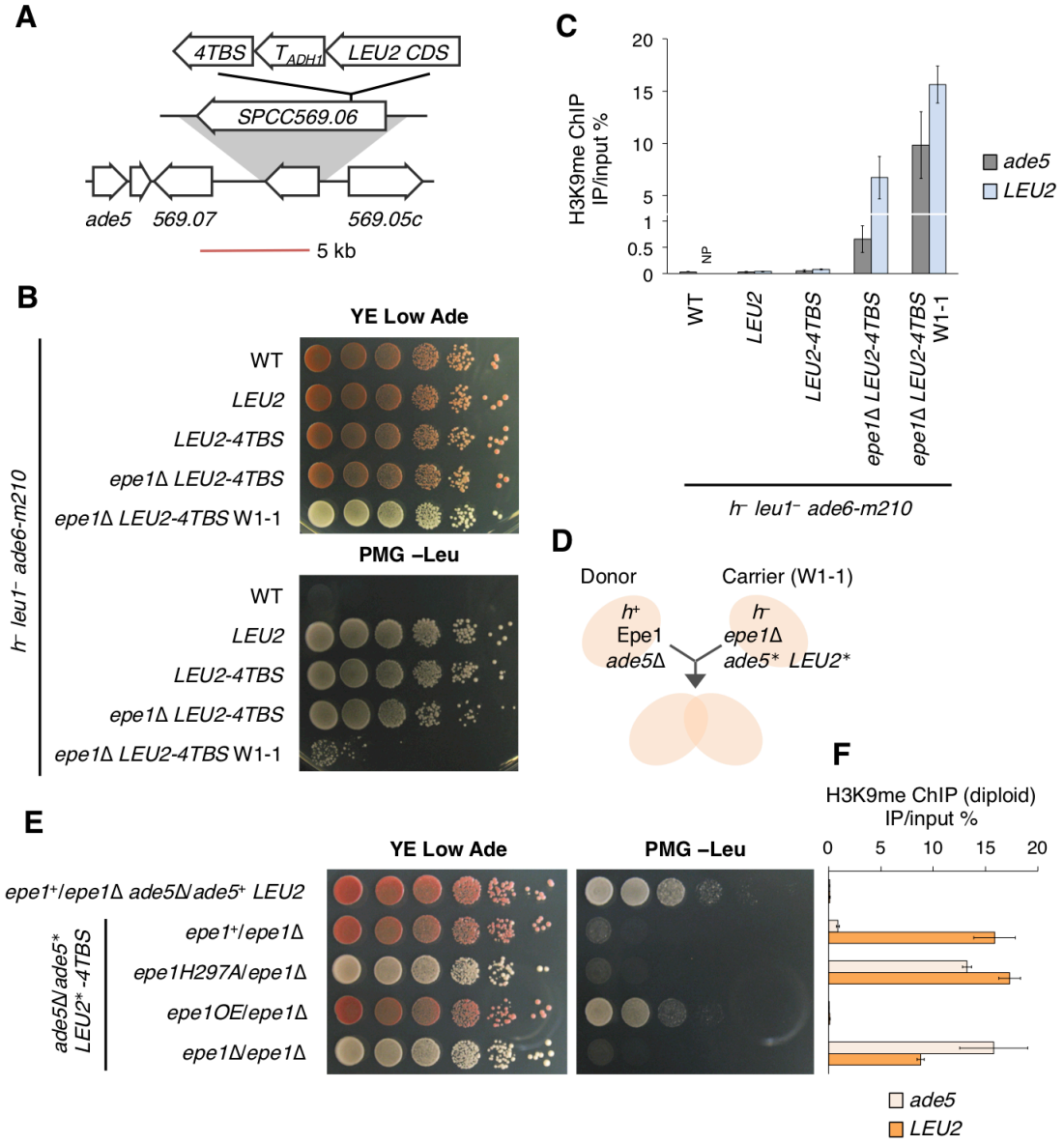

Figure 22. JmjC-mediated incomplete removal function allow retention of ectopic heterochromatin

(A) Schematic diagram of the *LEU2-4TBS* invasion system. Transcription of the coding sequence of *S. cerevisiae LEU2* was initiated by the promoter of *SPCC569.06* and terminated by the *S. cerevisiae ADH1* terminator. *4TBS* was placed after the terminator. Bar, 5 kb. (B) Ten-fold serial dilution assay of the strain harboring *4TBS*-induced heterochromatin shown on adenine-limited and PMG −Leu media. (C) ChIP-qPCR analysis of H3K9me at *ade5* and *LEU2*. NP, not performed. *4TBS* is about 1.3 and 9.5 kb away from the PCR loci of *LEU2* and *ade5*, respectively. (D) Schematic diagram of diploid complementation of *ade5** and *LEU2** epialleles. (E) Ten-fold serial dilution assay on adenine-limited and PMG −Leu media for diploid complementation. (F) ChIP-qPCR analysis of

H3K9me for diploid strains at *ade5* and *LEU2*. All strains provided monoallelic signals. ChIP-qPCR data in (C) and (F) are represented as mean ± standard deviation (SD) of three independent experiments (n = 3).

IV. Discussion

In this study, I demonstrated that Epe1 suppressed ectopic heterochromatin formation via two mechanisms as shown in Figure 23. First, Epe1 prevents the initial deposition of H3K9me at potential ectopic heterochromatin formation sites via a mechanism that does not require the function of its JmjC domain. Second, Epe1 promotes demethylation of H3K9me from established ectopic heterochromatin via a mechanism that requires its JmjC domain. These two distinct mechanisms cooperate to suppress ectopic heterochromatin formation. Loss of Epe1 induced stochastic accumulation of H3K9me, resulting in heterogeneous ectopic heterochromatin formation among clonal cells. Because constitutive supply of H3K9me antagonized the demethylation function of Epe1, some of the ectopic heterochromatin can be retained and provide a basis for epigenetic differences.

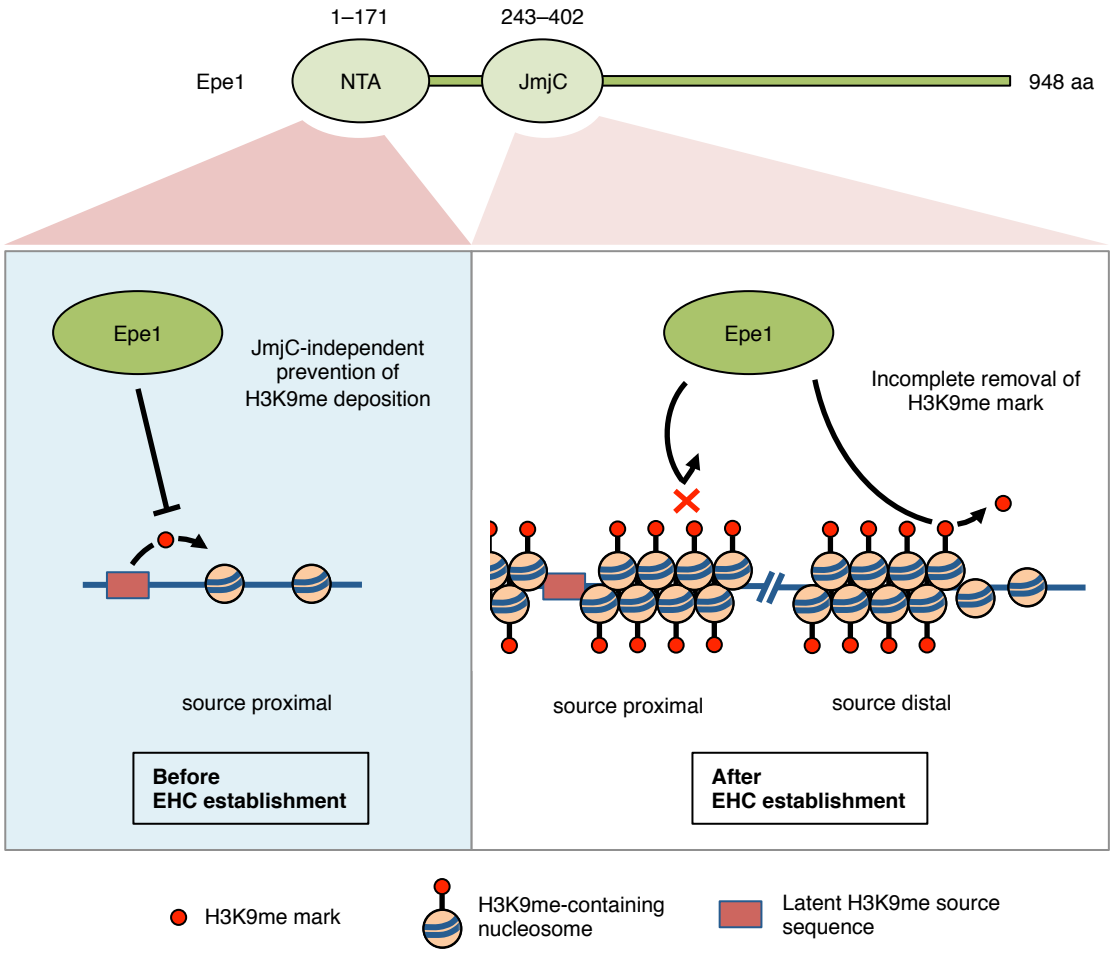

Figure 23. Model of two distinct functions of Epe1 in the suppression of ectopic heterochromatin formation and selective retention of robust ectopic heterochromatin

Before ectopic heterochromatin establishment (left), Epe1 prevents early deposition of H3K9me via a mechanism that involves its N-terminal transcriptional activation (NTA) domain but not its JmjC. After ectopic heterochromatin establishment (right), Epe1 promotes incomplete demethylation of ectopic H3K9me. Epe1 cannot disrupt already-established ectopic heterochromatin near an H3K9me supply source because the source provides H3K9me and counterbalances removal of H3K9me by Epe1, whereas Epe1 can remove the source-distal H3K9me mark in a JmjC-dependent manner. EHC, ectopic heterochromatin. NTA domain, 1–171 amino acid region as identified in this study; JmjC domain, 243–402 amino acid region as assigned in the SMART database (http://smart.embl-heidelberg.de).

IV-1. Loss of demethylase enhances stochastic formation of ectopic heterochromatin

ChIP-seq analysis revealed that each isolated clone of the *epe1*Δ strain had a unique H3K9me landscape. Thus, ectopic heterochromatin is formed stochastically and maintained stably, but its landscape occasionally shifts to another state. Therefore, I detected several metastable heterochromatin landscapes among *epe1*Δ isolates.

Ectopic heterochromatin formation at *ade5* and *gal1* associated with an increased level of H3K9me led to an alteration in phenotype, which clearly showed the gene silencing ability of ectopic heterochromatin. *gal1* ectopic heterochromatin seemed to be formed by spreading of subtelomeric heterochromatin of chromosome 2. On the other hand, it remains unknown how *ade5* ectopic heterochromatin is formed. It was established without RNAi or Taz1. In addition, *ade5* ectopic heterochromatin of the *epe1*Δ W1-1, W1-2, and W9-1 strains was not fused to rDNA heterochromatin. These results indicated that it was maintained independently of heterochromatin spreading from the right rDNA region. Note that it remains unclear whether *ade5* ectopic heterochromatin could be established without rDNA heterochromatin, because it is possible that heterochromatin at *SPCC569.03* and surrounding genes would regress after *subtel3R* ectopic heterochromatin was expanded from the rDNA region to *ade5*.

I found novel ectopic heterochromatin domains such as *clr2*, *pdi4*, *ade1*, and *can1* (Figure 10, 14, and 15), which appeared to have no identifiable H3K9me source, except for convergent genes [32, 68, 69, 76, 78, 84]. In addition, many ectopic heterochromatin domains identified in several mutant backgrounds have no known H3K9me source [68, 69, 72, 75]. These facts suggest that many potential H3K9me sources for heterochromatin formation exist in the genome and are incidentally activated to form ectopic heterochromatin in the absence of Epe1. Ectopic heterochromatin domains did not overlap with PIERs, but some of them were formed adjacent to an essential gene, consistent with PIERs [85]. RNA polymerase pausing is still a possible mechanism for inducing ectopic heterochromatin formation.

Loss of H3K9 demethylase in other organisms commonly alters traits by perturbing

the epigenomic state: in male mice, stochastic formation of testes, ovaries, and testis-ovary hybrids is induced by perturbations in the levels of histone modifications on the testis-determining gene *Sry* [96, 97]; and in *Arabidopsis*, a variety of developmental defects and genome-wide deposition of H3K9me and 5mC are observed [98, 99]. I further assume that loss of an H3K9 demethylase accelerates intratumoral heterogeneity, which interferes with chemotherapy by generating drug-tolerant subpopulations, because tumor evolution involves increases in repressive and decreases in active histone marks [100, 101], and co-dependency between genetic and epigenetic mutations possibly enhances the heterogeneity [102].

IV-2. Swi6-binding and heterochromatin association activities of Epe1 sense impairment of the N-terminal half region

The conserved histidine 297 in the JmjC domain, an important residue for Fe^{2+} binding, is essential for the promotion of H3K9 demethylation by Epe1 *in vivo* (Figure 19E) [56, 57]. Although *epe1H297A* cells largely maintained heterochromatin at *IRC3* and *dg*, Epe1H297A largely lost its heterochromatin localization (Figure 20C–E), indicating that histidine 297 was required for Epe1 localization to heterochromatin. I found that the H297A mutation slightly impaired the interaction of Epe1 with Swi6. This may not fully explain the reduced heterochromatin localization of Epe1 (Figure 20A). In contrast, in yeast two-hybrid assay, Swi6 interacted with the C-terminal half of Epe1, which lacks the JmjC domain, indicating that Epe1 has a Swi6 interaction site in its C-terminal half region (Figure 20B) [44]. Previous *in vitro* analysis shows that Swi6 interacts with a JmjC mutant, Epe1Y307A, which retains the metal-binding residues [43]. Thus, I speculate that conformational changes in the JmjC domain induced by perturbations in Fe^{2+} binding result in a slight alteration of the interaction surface for Swi6 binding, while severely disrupting the structure of a region essential for heterochromatin association. Heterochromatin association of Epe1 might require another mechanism in addition to its binding to Swi6. Moreover, Epe1ΔN–Swi6 interaction analysis revealed that lack of the NTA domain impaired the interaction of Epe1 with Swi6 (Figure 20A). It is possible that the N-terminal half region of Epe1 contributes to proper conformation for Epe1–Swi6 interaction and heterochromatin association.

IV-3. JmjC- and heterochromatin association-independent prevention

The JmjC mutant Epe1H297A almost completely suppressed the red-white variegation induced by ectopic heterochromatin assembly, while it failed to remove already-established ectopic heterochromatin (Figure 17B and 18E). Therefore, Epe1 prevents H3K9me deposition before the establishment of ectopic heterochromatin. Furthermore, the fact that Epe1H297A almost lacked heterochromatin association activity suggests that Epe1 recognizes potential ectopic heterochromatin formation sites in a manner distinct from heterochromatin targeting. However, the recognition mechanism is unclear at this stage.

The newly identified NTA domain showed transcriptional activation ability in both budding and fission yeasts (Figure 19A and 19B), indicating that the NTA domain functions as a conserved transcriptional activation domain like VP16 TAD to recruit RNA polymerase II. Accordingly, Epe1 interacts with a histone acetyltransferase complex, SAGA, which is involved in transcriptional activation [66]. Importantly, loss of the NTA domain induced a variegation phenotype (Figure 19C). These results raise the possibility that the transcriptional activation activity of Epe1 is involved in the prevention of H3K9me deposition. Recent reports show that loss of Leo1, a component of the transcription elongation complex Paf1C, causes ectopic heterochromatin formation [72, 73, 74]. Similarly, loss of Mst2, a histone acetyltransferase, induces ectopic heterochromatin formation [69]. Importantly, loss of each of these proteins causes a decrease in histone turnover [69, 74]. Since histone turnover is associated with transcription [74, 103] and Epe1 promotes histone turnover in heterochromatin [67], Epe1 might exclude H3K9me-containing nucleosomes by activating histone turnover coupled with transcriptional activation at the potential ectopic heterochromatin formation sites.

It is still possible that the NTA domain has a function, other than transcriptional activation, which contributes to the prevention of ectopic heterochromatin formation. I found that lack of the NTA domain impaired the interaction of Epe1 with Swi6 (Figure 20A). Heterochromatin association is not required for the prevention of ectopic

H3K9me deposition as described above, but Epe1–Swi6 interaction might contribute to the prevention through a mechanism independent of heterochromatin association. Further studies such as determination of important amino acids for the transcriptional activation and interaction with Swi6 will clarify the mechanism of JmjC-independent prevention.

IV-4. An Epe1-mediated mechanism for producing variation of the H3K9me landscape

I found that re-introduction of single copy Epe1 did not erase ectopic heterochromatin when an H3K9me source existed nearby, while Epe1 overexpression completely erased it. On the other hand, increased levels of Epe1 impair constitutive heterochromatin [43, 45, 63]. The expression level of endogenous Epe1 appears to be appropriately regulated to allow ectopic heterochromatin retention while keeping constitutive heterochromatin intact. Since Epe1 is degraded in S phase by the Cul4-Ddb1^{Cdt2} complex [63] and phosphorylation of Swi6 affects localization of Epe1 to heterochromatin [60], I assume that transient inactivation, loss of expression, or delocalization of Epe1 provides an opportunity to change the heterochromatin landscape. Differences in the H3K9me landscape between wild-type strains might reflect transient changes in Epe1 activity (Figure 13A and 16). Recently, Gallagher et al. reported that low temperature induces the formation of additional heterochromatin islands including *SPCC569.03* [71], where I found robust ectopic heterochromatin that tolerated the re-introduction of a single copy of *epe1*$^{+}$ (Figure 21). This emergence of islands might be caused by impaired Epe1 function at low temperatures. Such regulatory mechanisms appear to be widely applicable to organisms that have demethylases that erase repressive histone methyl marks. Although the genome contains numerous potentially H3K9me-inducible sequences [79, 104, 105], not all of them exhibit H3K9me accumulation. Ectopic heterochromatin formation at these sequences, inducible under specific conditions, might result in unprogrammed epigenetic differences.

Variation of the H3K9me landscape could produce adaptive subpopulations, because the variation could switch metabolic pathways or induce changes in growth to those suited for survival in a particular environment [106]. Indeed, ectopic heterochromatin

affects ribonucleotide synthesis (*ade5* and *ade1*) and carbon source metabolism (*gal1*). This study provides insights into the mechanisms of epigenetic diversification and maintenance, which underlie cellular homeostasis and heterogeneous evolution.

V. Conclusion

It was believed that red-white variegation in the loss of *epe1* reflects heterogeneous expression of the centromeric *ade6* marker gene [44], but I showed that stochastic ectopic heterochromatin formation at pigmentation-related genes is also responsible for variegation. Genome-wide analysis in isolated *epe1*-null clones revealed a dynamic change in the form of subtelomeric ectopic heterochromatin and the heterogeneous appearance of ectopic heterochromatin among clonal cells, suggesting that the epigenome potentially diversifies to form individual-specific phenotypes, which is suppressed by Epe1. Epe1H297A suppressed variegation, which distinguished prevention of ectopic H3K9me deposition from removal of H3K9me from already-established heterochromatin. Although previous studies, using an artificial heterochromatin construction system, suggested that Epe1 promotes JmjC-mediated removal of euchromatic H3K9me [56, 57], I found a novel domain, NTA, which contributes to prevention of ectopic heterochromatin formation in a JmjC-independent mechanism. Re-introduction of Epe1 into ectopic heterochromatin-bearing *epe1*Δ cells revealed regions where H3K9me persisted. This suggests that the function of Epe1 to counteract H3K9me is not exhaustive, which can produce a different epigenetic state of the strain that experienced loss and gain of *epe1* from that of the wild-type strain despite having isogenic genotypes. Epe1 plays a key role in the control of homeostasis and plasticity of the epigenetic state.

VI. References

1. Luger K, Dechassa ML, Tremethick DJ. New insights into nucleosome and chromatin structure: an ordered state or a disordered affair? Nat Rev Mol Cell Biol. 2012;13(7):436–447.

2. Mcginty RK, Tan S. Nucleosome structure and function. Chem Rev. 2015;115(6):2255–2273.

3. Jenuwein T, Allis CD. Translating the histone code. Science. 2001;293(5532):1074–1080.

4. Zhao Y, Garcia BA. Comprehensive catalog of currently documented histone modifications. Cold Spring Harb Perspect Biol. 2015;7(9):a025064

5. Talbert PB, Henikoff S. Spreading of silent chromatin: inaction at a distance. Nat Rev Genet. 2006;7(10):793–803.

6. Grewal SIS, Jia S. Heterochromatin revisited. Nat Rev Genet. 2007;8(1):35–46.

7. Allshire RC, Madhani HD. Ten principles of heterochromatin formation and function. Nat Rev Mol Cell Biol. 2018;19(4):229–244.

8. Heard E, Martienssen RA. Transgenerational epigenetic inheritance: Myths and mechanisms. Cell. 2014;157(1):95–109.

9. Rea S, Eisenhaber F, O'Carroll D, Strahl BD, Sun ZW, Schmid M, et al. Regulation of chromatin structure by site-specific histone H3 methyltransferases. Nature. 2000;406(6796):593–599.

10. Nakayama J-I, Rice JC, Strahl BD, Allis CD, Grewal SIS. Role of Histone H3 Lysine 9 Methylation in Epigenetic Control of Heterochromatin Assembly. Science. 2001;292(5514):110–113.

11. Cam HP, Sugiyama T, Chen ES, Chen X, FitzGerald PC, Grewal SIS. Comprehensive analysis of heterochromatin- and RNAi-mediated epigenetic control of the fission yeast genome. Nat Genet. 2005;37(8):809–819.

12. Volpe TA, Kidner C, Hall IM, Teng G, Grewal SIS, Martienssen RA. Regulation of heterochromatic silencing and histone H3 lysine-9 methylation by RNAi. Science. 2002;297(5588):1833–1837.

13. Castel SE, Martienssen RA. RNA interference in the nucleus: roles for small RNAs in transcription, epigenetics and beyond. Nat Rev Genet. 2013;14(2):100–112.

14. Holoch D, Moazed D. RNA-mediated epigenetic regulation of gene expression. Nat Rev Genet. 2015;16(2):71–84.

15. Kato H, Goto DB, Martienssen RA, Urano T, Furukawa K, Murakami Y. RNA polymerase II is required for RNAi-dependent heterochromatin assembly. Science. 2005;309(5733):467–469.

16. Djupedal I, Portoso M, Spåhr H, Bonilla C, Gustafsson CM, Allshire RC, et al. RNA Pol II subunit Rpb7 promotes centromeric transcription and RNAi-directed chromatin silencing. Genes Dev. 2005;19(19):2301–2306.

17. Djupedal I, Kos-Braun IC, Mosher RA, Söderholm N, Simmer F, Hardcastle TJ, et al. Analysis of small RNA in fission yeast; centromeric siRNAs are potentially generated through a structured RNA. EMBO J. 2009;28(24):3832–3844.

18. Motamedi MR, Verdel A, Colmenares SU, Gerber SA, Gygi SP, Moazed D. Two RNAi Complexes, RITS and RDRC, Physically Interact and Localize to Noncoding Centromeric RNAs. Cell. 2004;119(6):789–802.

19. Kawakami K, Hayashi A, Nakayama J-I, Murakami Y. A novel RNAi protein, Dsh1, assembles RNAi machinery on chromatin to amplify heterochromatic siRNA. Genes Dev. 2012;26(16):1811–1824.

20. Verdel A, Jia S, Gerber S, Sugiyama T, Gygi S, Grewal SIS, et al. RNAi-Mediated Targeting of Heterochromatin by the RITS. Science. 2004;303(5658):672–676

21. Kajitani T, Kato H, Chikashige Y, Tsutsumi C, Hiraoka Y, Kimura H, et al. Ser7 of RNAPII-CTD facilitates heterochromatin formation by linking ncRNA to RNAi. Proc Natl Acad Sci. 2017;114(52):E11208–11217.

22. Hong EJE, Villén J, Gerace EL, Gygi SP, Moazed D. A cullin E3 ubiquitin ligase complex associates with Rik1 and the Clr4 histone H3-K9 methyltransferase and is required for RNAi-mediated heterochromatin formation. RNA Biol. 2005;2(3):106–111.

23. Kuscu C, Zaratiegui M, Kim HS, Wah DA, Martienssen RA, Schalch T, et al. CRL4-like Clr4 complex in Schizosaccharomyces pombe depends on an exposed surface of Dos1 for heterochromatin silencing. Proc Natl Acad Sci U S A. 2014;111(5):1795–1800.

24. Bayne EH, White S a., Kagansky A, Bijos DA., Sanchez-Pulido L, Hoe KL, et al. Stc1: A Critical Link between RNAi and Chromatin Modification Required for Heterochromatin Integrity. Cell. 2010;140(5):666–677.

25. Zhang K, Mosch K, Fischle W, Grewal SIS. Roles of the Clr4 methyltransferase complex in nucleation, spreading and maintenance of heterochromatin. Nat Struct Mol Biol. 2008;15(4):381–388.

26. Reyes-Turcu FE, Zhang K, Zofall M, Chen E, Grewal SIS. Defects in RNA quality control factors reveal RNAi-independent nucleation of heterochromatin. Nat Struct Mol Biol. 2011;18(10):1132–1138.

27. Oya E, Kato H, Chikashige Y, Tsutsumi C, Hiraoka Y, Murakami Y. Mediator Directs Co-transcriptional Heterochromatin Assembly by RNA Interference-Dependent and -Independent Pathways. PLoS Genet. 2013;9(8):e1003677.

28. Chalamcharla VR, Folco HD, Dhakshnamoorthy J, Grewal SIS. Conserved factor Dhp1/Rat1/Xrn2 triggers premature transcription termination and nucleates heterochromatin to promote gene silencing. Proc Natl Acad Sci. 2015;112(51):15548–15555.

29. Kanoh J, Sadaie M, Urano T, Ishikawa F. Telomere binding protein Taz1 establishes Swi6 heterochromatin independently of RNAi at telomeres. Curr Biol. 2005;15(20):1808–19.

30. Miyoshi T, Kanoh J, Saito M, Ishikawa F. Fission yeast pot1-Tpp1 protects telomeres and regulates telomere length. Science. 2008;320(5881):1341–4.

31. Wang J, Cohen AL, Letian A, Tadeo X, Moresco JJ, Liu J, et al. The proper connection between shelterin components is required for telomeric heterochromatin assembly. Genes Dev. 2016;30(7):827–839.

32. Zofall M, Smith DR, Mizuguchi T, Dhakshnamoorthy J, Grewal SIS. Taz1-Shelterin Promotes Facultative Heterochromatin Assembly at Chromosome-Internal Sites Containing Late Replication Origins. Mol Cell. 2016;62(6):862–874.

33. Thon G, Verhein-Hansen J. Four chromo-domain proteins of Schizosaccharomyces pombe differentially repress transcription at various chromosomal locations. Genetics. 2000;155(2):551–568.

34. Jakociunas T, Domange Jordö M, Aït Mebarek M, Bünner CM, Verhein-Hansen J, Oddershede LB, et al. Subnuclear relocalization and silencing of a chromosomal region by an ectopic ribosomal DNA repeat. Proc Natl Acad Sci U S A. 2013;110(47):E4465–4473.

35. Sugiyama T, Thillainadesan G, Chalamcharla VR, Meng Z, Balachandran V, Dhakshnamoorthy J, et al. Enhancer of Rudimentary Cooperates with Conserved RNA-Processing Factors to Promote Meiotic mRNA Decay and Facultative Heterochromatin Assembly. Mol Cell. 2016;61(5):747–759.

36. Takeda T, Toda T, Kominami K, Kohnosu a, Yanagida M, Jones N. Schizosaccharomyces pombe atf1+ encodes a transcription factor required for sexual development and entry into stationary phase. EMBO J. 1995;14(24):6193–6208.

37. Jia S, Noma K, Grewal SIS. RNAi-independent heterochromatin nucleation by the stress-activated ATF/CREB family proteins. Science. 2004;304(5679):1971–1976.

38. Kim HS, Choi ES, Shin JA, Jang YK, Park SD. Regulation of Swi6/HP1-dependent heterochromatin assembly by cooperation of components of the mitogen-activated protein kinase pathway and a histone deacetylase Clr6. J Biol Chem. 2004;279(41):42850–42859.

39. Allshire RC, Javerzat JP, Redhead NJ, Cranston G. Position effect variegation at fission yeast centromeres. Cell. 1994;76(1):157–169.

40. Allshire RC, Nimmo ER, Ekwall K, Javerzat JP, Cranston G. Mutations derepressing silent centromeric domains in fission yeast disrupt chromosome segregation. Genes Dev. 1995;9(2):218–233.

41. Ekwall K, Olsson T, Turner BM, Cranston G, Allshire RC. Transient inhibition of histone deacetylation alters the structural and functional imprint at fission yeast centromeres. Cell. 1997;91(7):1021–1032.

42. Ayoub N, Noma K, Isaac S, Kahan T, Grewal SIS., Cohen A. A Novel jmjC Domain Protein Modulates Heterochromatization in Fission Yeast. Mol Cell Biol. 2003; 23:4356–4370

43. Zofall M, Grewal SIS. Swi6/HP1 recruits a JmjC domain protein to facilitate transcription of heterochromatic repeats. Mol Cell. 2006;22(5):681–692.

44. Trewick SC, Minc E, Antonelli R, Urano T, Allshire RC. The JmjC domain protein Epe1 prevents unregulated assembly and disassembly of heterochromatin. EMBO J. 2007;26(22):4670–4682.

45. Isaac S, Walfridsson J, Zohar T, Lazar D, Kahan T, Ekwall K, et al. Interaction of Epe1 with the heterochromatin assembly pathway in Schizosaccharomyces pombe. Genetics. 2007;175(4):1549–1560.

46. Tsukada Y, Fang J, Erdjument-Bromage H, Warren ME, Borchers CH, Tempst P, et al. Histone demethylation by a family of JmjC domain-containing proteins. Nature. 2006;439(7078):811–816.

47. Shinkai Y, Tachibana M. H3K9 methyltransferase G9a and the related molecule GLP. Genes Dev. 2011;25(8):781–788.

48. Klose RJ, Kallin EM, Zhang Y. JmjC-domain-containing proteins and histone demethylation. Nat Rev Genet. 2006;7(9):715–27.

49. Allis CD, Berger SL, Cote J, Dent S, Jenuwien T, Kouzarides T, et al. New Nomenclature for Chromatin-Modifying Enzymes. Cell. 2007;131(4):633–636.

50. Cloos PA, Christensen J, Agger K, Helin K. Erasing the methyl mark: Histone demethylases at the center of cellular differentiation and disease. Genes Dev. 2008;22(9):1115–1140.

51. Trewick SC, McLaughlin PJ, Allshire RC. Methylation: lost in hydroxylation? EMBO Rep. 2005;6(4):315–320.

52. Wen H, Li J, Song T, Lu M, Kan PY, Lee MG, et al. Recognition of histone H3K4 trimethylation by the plant homeodomain of PHF2 modulates histone demethylation. J Biol Chem. 2010;285(13):9322–9326.

53. Horton JR, Upadhyay AK, Hashimoto H, Zhang X, Cheng X. Structural basis for human PHF2 Jumonji domain interaction with metal ions. J Mol Biol. 2011;406(1):1–8.

54. Baba A, Ohtake F, Okuno Y, Yokota K, Okada M, Imai Y, et al. PKA-dependent regulation of the histone lysine demethylase complex PHF2-ARID5B. Nat Cell Biol. 2011;13(6):668–675.

55. Lal S, Comer JM, Konduri PC, Shah A, Wang T, Lewis A, et al. Heme promotes transcriptional and demethylase activities of Gis1, a member of the histone demethylase JMJD2/KDM4 family. Nucleic Acids Res. 2017;46(1):215–228.

56. Ragunathan K, Jih G, Moazed D. Epigenetic inheritance uncoupled from sequence-specific recruitment. Science. 2015;1258699.

57. Audergon PNCB, Catania S, Kagansky A, Tong P, Shukla M, Pidoux AL, et al. Epigenetics. Restricted epigenetic inheritance of H3K9 methylation. Science. 2015;348(6230):132–135.

58. Seo HD, Choi Y, Kim M, Kang K, Urano T, Lee D. The 19S proteasome is directly involved in the regulation of heterochromatin spreading in fission yeast. J Biol Chem. 2017;292(41):17144–17155.

59. Sadaie M, Kawaguchi R, Ohtani Y, Arisaka F, Tanaka K, Shirahige K, et al. Balance between distinct HP1 family proteins controls heterochromatin assembly in fission yeast. Mol Cell Biol. 2008;28(23):6973–6988.

60. Shimada A, Dohke K, Sadaie M, Shinmyozu K, Nakayama J-I, Urano T, et al. Phosphorylation of Swi6/HP1 regulates transcriptional gene silencing at heterochromatin. Genes Dev. 2009;23(1):18–23.

61. Noma K, Allis CD, Grewal SIS. Transitions in distinct histone H3 methylation patterns at the heterochromatin domain boundaries. Science. 2001;293(5532):1150–1155.

62. Noma K, Cam HP, Maraia RJ, Grewal SIS. A role for TFIIIC transcription factor complex in genome organization. Cell. 2006;125(5):859–872.

63. Braun S, Garcia JF, Rowley M, Rougemaille M, Shankar S, Madhani HD. The Cul4-Ddb1(Cdt)^2 ubiquitin ligase inhibits invasion of a boundary-associated antisilencing factor into heterochromatin. Cell. 2011;144(1):41–54.

64. Wang J, Tadeo X, Hou H, Tu PG, Thompson J, Yates JR, et al. Epe1 recruits BET family bromodomain protein Bdf2 to establish heterochromatin boundaries. Genes Dev. 2013;27(17):1886–1902.

65. Keller C, Kulasegaran-Shylini R, Shimada Y, Hotz H-R, Bühler M. Noncoding RNAs prevent spreading of a repressive histone mark. Nat Struct Mol Biol. 2013;20(8):994–1000.

66. Bao K, Shan CM, Moresco J, Yates J, Jia S. Anti-silencing factor Epe1 associates with SAGA to regulate transcription within heterochromatin. Genes Dev. 2019;33(1–2):116–126.

67. Aygün O, Mehta S, Grewal SIS. HDAC-mediated suppression of histone turnover promotes epigenetic stability of heterochromatin. Nat Struct Mol Biol. 2013;20(5):547–554.

68. Zofall M, Yamanaka S, Reyes-Turcu FE, Zhang K, Rubin C, Grewal SIS. RNA elimination machinery targeting meiotic mRNAs promotes facultative heterochromatin formation. Science. 2012;335(6064):96–100.

69. Wang J, Reddy BD, Jia S. Rapid epigenetic adaptation to uncontrolled heterochromatin spreading. Elife. 2015;4:e06179.

70. Tashiro S, Asano T, Kanoh J, Ishikawa F. Transcription-induced chromatin association of RNA surveillance factors mediates facultative heterochromatin formation in fission yeast. Genes to Cells. 2013;18(4):327–339.

71. Gallagher PS, Larkin M, Thillainadesan G, Dhakshnamoorthy J, Balachandran V, Xiao H, et al. Iron homeostasis regulates facultative heterochromatin assembly in adaptive genome control. Nat Struct Mol Biol. 2018;25(5):372–383.

72. Seo HD, Kwon CS, Lee D. The 19S proteasome regulates subtelomere silencing and facultative heterochromatin formation in fission yeast. Curr Genet. 2018;64(3):741–752.

73. Verrier L, Taglini F, Barrales RR, Webb S, Urano T, Braun S, et al. Global regulation of heterochromatin spreading by Leo1. Open Biol. 2015;5:150045

74. Sadeghi L, Prasad P, Ekwall K, Cohen A, Svensson JP. The Paf1 complex factors Leo1 and Paf1 promote local histone turnover to modulate chromatin states in fission yeast. EMBO Rep. 2015;16(12):1673–1687.

75. Iglesias N, Currie MA, Jih G, Paulo JA, Siuti N, Kalocsay M, et al. Automethylation-induced conformational switch in Clr4 (Suv39h) maintains epigenetic stability. Nature. 2018;560(7719):504–508.

76. Gullerova M, Proudfoot NJ. Cohesin Complex Promotes Transcriptional Termination between Convergent Genes in S. pombe. Cell. 2008;132(6):983–995.

77. Yu R, Jih G, Iglesias N, Moazed D. Determinants of Heterochromatic siRNA Biogenesis and Function. Mol Cell. 2013;1–15.

78. Yamanaka S, Mehta S, Reyes-Turcu FE, Zhuang F, Fuchs RT, Rong Y, et al. RNAi triggered by specialized machinery silences developmental genes and retrotransposons. Nature. 2013;493(7433):557–560.

79. Harigaya Y, Tanaka H, Yamanaka S, Tanaka K, Watanabe Y, Tsutsumi C, et al. Selective elimination of messenger RNA prevents an incidence of untimely meiosis. Nature. 2006;442(7098):45–50.

80. Yamashita A, Shichino Y, Tanaka H, Hiriart E, Touat-Todeschini L, Vavasseur A, et al. Hexanucleotide motifs mediate recruitment of the RNA elimination machinery to silent meiotic genes. Open Biol. 2012;2(3):120014.

81. Hiriart E, Vavasseur A, Touat-Todeschini L, Yamashita A, Gilquin B, Lambert E, et al. Mmi1 RNA surveillance machinery directs RNAi complex RITS to specific meiotic genes in fission yeast. EMBO J. 2012;31(10):2296–308.

82. Lee NN, Chalamcharla VR, Reyes-Turcu F, Mehta S, Zofall M, Balachandran V, et al. Mtr4-like Protein Coordinates Nuclear RNA Processing for Heterochromatin Assembly and for Telomere Maintenance. Cell. 2013;155(5):1061–1074.

83. Egan ED, Braun CR, Gygi SP, Moazed D. Post-transcriptional regulation of meiotic genes by a nuclear RNA silencing complex. 2014;2014:867–881.

84. Shah S, Wittmann S, Kilchert C, Vasiljeva L. lncRNA recruits RNAi and the exosome to dynamically regulate pho1 expression in response to phosphate levels in fission yeast. Genes Dev. 2014;28(3):231–244.

85. Parsa JY, Boudoukha S, Burke J, Homer C, Madhani HD. Polymerase pausing induced by sequence-specific RNA-binding protein drives heterochromatin assembly. Genes Dev. 2018;32(13–14):953–964.

86. Moreno S, Klar A, Nurse P. Molecular genetic analysis of fission yeast Schizosaccharomyces pombe. Methods Enzymol. 1991;194:795–823.

87. Sabatinos SA, Forsburg SL. Molecular genetics of schizosaccharomyces pombe. Methods in Enzymology 2010;470:759–795.

88. Bähler J, Wu JQ, Longtine MS, Shah NG, McKenzie A, Steever AB, et al. Heterologous modules for efficient and versatile PCR-based gene targeting in Schizosaccharomyces pombe. Yeast. 1998;14(10):943–951.

89. Cooper JP, Nimmo ER, Allshire RC, Cech TR. Regulation of telomere length and function by a Myb-domain protein in fission yeast. Nature. 1997;385(6618):744–747.

90. Spink KG, Evans RJ, Chambers A. Sequence-specific binding of Taz1p dimers to fission yeast telomeric DNA. Nucleic Acids Res. 2000;28(2):527–533.

91. Matsuda A, Chikashige Y, Ding D-Q, Ohtsuki C, Mori C, Asakawa H, et al. Highly condensed chromatins are formed adjacent to subtelomeric and decondensed silent chromatin in fission yeast. Nat Commun. 2015;6:7753.

92. Kimura H, Hayashi-Takanaka Y, Goto Y, Takizawa N, Nozaki N. The organization of histone H3 modifications as revealed by a panel of specific monoclonal antibodies. Cell Struct Funct. 2008;33(1):61–73.

93. Nakayama J-I, Klar AJ, Grewal SIS. A Chromodomain Protein, Swi6, Performs Imprinting Functions in Fission Yeast during Mitosis and Meiosis. Cell. 2000;101(3):307–317.

94. Schweingruber ME, Zurlinden A. Identification of a DNA Element in the Fission Yeast *Schizosaccharomyces pombe nmt1* (*thi3*) Promoter Involved in Thiamine-Regulated Gene Expression. J Bacteriol. 1997;179(18):5956–5958.

95. Forsburg SL, Sherman DA. General purpose tagging vectors for fission yeast. Gene. 1997;191(2):191–195.

96. Kuroki S, Matoba S, Akiyoshi M, Matsumura Y, Miyachi H, Mise N, et al. Epigenetic regulation of mouse sex determination by the histone demethylase Jmjd1a. Science. 2013;341(6150):1106–1109.

97. Kuroki S, Okashita N, Baba S, Maeda R, Miyawaki S, Yano M, et al. Rescuing the aberrant sex development of H3K9 demethylase Jmjd1a-deficient mice by modulating H3K9 methylation balance. PLoS Genet. 2017;13(9):1–22.

98. Saze H, Shiraishi A, Miura A, Kakutani T. Control of genic DNA methylation by a jmjC domain-containing protein in Arabidopsis thaliana. Science. 2008;319(5862):462–465.

99. Inagaki S, Miura-Kamio A, Nakamura Y, Lu F, Cui X, Cao X, et al. Autocatalytic differentiation of epigenetic modifications within the Arabidopsis genome. EMBO J. 2010;29(20):3496–3506.

100. Sharma SV, Lee DY, Li B, Quinlan MP, Takahashi F, Maheswaran S, et al. A Chromatin-Mediated Reversible Drug-Tolerant State in Cancer Cell Subpopulations. Cell. 2010;141(1):69–80.

101. Guler GD, Tindell CA, Pitti R, Wilson C, Nichols K, KaiWai Cheung T, et al. Repression of Stress-Induced LINE-1 Expression Protects Cancer Cell Subpopulations from Lethal Drug Exposure. Cancer Cell. 2017;32(2):221–237.

102. Mazor T, Pankov A, Song JS, Costello JF. Intratumoral Heterogeneity of the Epigenome. Cancer Cell. 2016;29(4):440–451.

103. Venkatesh S, Workman JL. Histone exchange, chromatin structure and the regulation of transcription. Nat Rev Mol Cell Biol. 2015;16(3):178–189.

104. Eshaghi M, Lee JH, Zhu L, Poon SY, Li J, Cho KH, et al. Genomic binding profiling of the fission yeast stress-activated MAPK sty1 and the bZIP transcriptional activator Atf1 in response to H2O2. PLoS One. 2010;5(7).

105. Tazumi A, Fukuura M, Nakato R, Kishimoto A, Takenaka T, Ogawa S, et al. Telomere-binding protein Taz1 controls global replication timing through its localization near late replication origins in fission yeast. Genes Dev. 2012;26(18):2050–2062.

106. Chen Y, Hu X, Guo C, Yu Y, Lu H. Epe1 contributes to activation of AMPK by promoting phosphorylation of AMPK alpha subunit, Ssp2. Sci Rep.

Acknowledgements

First of all, I would like to express my sincere gratitude to my supervisor Professor Yota Murakami for his encouragement, extensive discussions, and broad mind.

I would like to thank the thesis committee members, Professor Kazuyasu Sakaguchi, Professor Yasuyuki Fujita, Professor Akinori Takaoka, and Professor Ken'ichiro Matsumoto for their valuable suggestions on my PhD work.

I would like to express my gratitude to Assistant Professor Shinya Takahata for his mentoring and technical support. I would like to express my appreciation to Associate Professor Masayuki Takahashi and Associate Professor Akiko Nakatomi for their kind guidance and suggestions. I also appreciate all the previous and current members of Laboratory of Bioorganic chemistry, especially Dr. Atsushi Shimada, Mr. Takahiro Hirauchi, Mr. Hiroaki Ishizaki, Mr. Michiaki Sato, and Mr. Wataru Kaito for their contribution to this work and Dr. Takuya Kajitani and Mr. Takahiro Asanuma for their advice throughout my study.

I am grateful to the collaborators, Assistant Professor Hiroaki Kato (Shimane University School of Medicine) for his guidance in analysis of transcriptome and ChIP-seq data, Dr. Yuji Chikashige (Senior Researcher of NICT) and Professor Yasushi Hiraoka (Osaka University) for transcriptome analysis, Professor Yasuyuki Ohkawa (Kyusyu University) and Professor Yutaka Suzuki (The University of Tokyo) for ChIP-seq analysis, Professor Takeshi Urano (Shimane University School of Medicine) for providing H3K9me antibody, and Professor Hiroshi Kimura (Tokyo Institute of Technology) for providing the H3K9me2 and me3 antibodies.

Finally, I would like to thank my parents for their prolonged financial support and my family and long-time friends for their encouragement.